

LA-UR-15-27788 (Accepted Manuscript)

Correlated Pc4-5 ULF waves, whistler-mode chorus, and pulsating aurora observed by the Van Allen Probes and ground-based systems

Jaynes, A.; Lessard, M.; Takahashi, K.; Ali, A.; Malaspina, D.; Mitchell, R.; Spanswick, E.; Baker, D.; Blake, J.; Cully, C.; Donovan, E.; Kletzing, C.; Reeves, Geoffrey D.; Samara, M.; Spence, H.; Wygant, J.

Provided by the author(s) and the Los Alamos National Laboratory (2016-06-22).

To be published in: Journal of Geophysical Research: Space Physics

DOI to publisher's version: 10.1002/2015JA021380

Permalink to record: <http://permalink.lanl.gov/object/view?what=info:lanl-repo/lareport/LA-UR-15-27788>

Disclaimer:

Approved for public release. Los Alamos National Laboratory, an affirmative action/equal opportunity employer, is operated by the Los Alamos National Security, LLC for the National Nuclear Security Administration of the U.S. Department of Energy under contract DE-AC52-06NA25396. Los Alamos National Laboratory strongly supports academic freedom and a researcher's right to publish; as an institution, however, the Laboratory does not endorse the viewpoint of a publication or guarantee its technical correctness.

1 Correlated Pc4-5 ULF waves, whistler-mode chorus
2 and pulsating aurora observed by the Van Allen
3 Probes and ground-based systems

A. N. Jaynes¹, M. R. Lessard², K. Takahashi³, A. F. Ali¹, D. M. Malaspina¹,
R. G. Michell^{4,5}, E. L. Spanswick⁶, D. N. Baker¹, J. B. Blake⁷, C. Cully⁶, E.
F. Donovan⁶, C. A. Kletzing⁸, G. D. Reeves^{9,10}, M. Samara⁵, H. E. Spence²,
and J. R. Wygant¹¹

¹Laboratory for Atmospheric and Space

Abstract. Theory and observations have linked equatorial VLF waves with pulsating aurora for decades, invoking the process of pitch-angle scattering of 10's keV electrons in the equatorial magnetosphere. Recently published satellite studies have strengthened this argument, by showing strong correlation between pulsating auroral patches and both lower-band chorus and 10's keV electron modulation in the vicinity of geosynchronous orbit. Additionally, a previous link has been made between Pc4-5 compressional pulsations and modulation of whistler-mode chorus using THEMIS. In the current study, we present simultaneous in-situ observations of structured chorus waves and an apparent field line resonance (in the Pc4-5 range) as a result of a substorm injection, observed by Van Allen Probes, along with ground-based observations of pulsating aurora. We demonstrate the likely scenario being one of substorm-driven Pc4-5 ULF pulsations modulating chorus waves, and thus providing the driver for pulsating particle precipitation into the Earth's atmosphere. Interestingly, the modulated chorus wave and ULF wave periods are well correlated, with chorus occurring at half the periodicity of the ULF waves. We also show, for the first time, a particular few-Hz modulation of individual chorus elements that coincides with the same modulation in a nearby pulsating aurora patch. Such modulation has been noticed as a high-frequency component in ground-based camera data of pulsating aurora for decades, and may be a result of nonlinear chorus wave interactions in the equatorial region.

Physics, University of Colorado, Boulder,

Colorado

²University of New Hampshire, Space
Science Center, New Hampshire

³JHU/APL, Laurel, Maryland

⁴University of Maryland, College Park,
Maryland

⁵Division of Heliophysics, NASA GSFC,
Greenbelt, Maryland

⁶University of Calgary, Calgary, Alberta,
Canada.

⁷Aerospace Corporation, El Segundo,
California

⁸University of Iowa, Iowa City, Iowa

⁹Los Alamos National Laboratory, Los
Alamos, New Mexico

¹⁰New Mexico Consortium, Los Alamos,
New Mexico

¹¹University of Minnesota, Minneapolis,
Minnesota

1. Introduction

Many disparate studies have been carried out that link one to another of the following series of events: substorm injections into the inner magnetosphere, Pc4-5 ULF wave excitation, modulation of VLF chorus, and precipitation via scattering in the form of modulated pulsating aurora (PA). Using the new perspective gained with the high-fidelity measurements onboard the Van Allen Probes, in conjunction with ground-based imagers, we show that the processes in these events are highly connected. In this paper, we present a case study of this sequence as a cohesive narrative, with implications for future magnetospheric studies of these phenomena.

1.1. Pulsating aurora

PA is a distinct type of periodically modulated aurora, which is manifest as diffuse patches characterized by quasi-periodic brightness fluctuations of ~ 2 -20 second periods, and horizontal sizes of several to hundreds of kilometers [Johnstone, 1978]. Nearby patches can pulsate out of phase or entirely independently of one another, indicating that the temporal variation of PA can change dramatically from one patch to the next [Omholt, 1971; Royrvik and Davis, 1977; Smith et al., 1980; Duncan et al., 1981]. The brightness of the patches is only a few hundred Rayleigh (R) to a few kR at 428 nm, and normally occurs over a diffuse background [Royrvik and Davis, 1977], with maximum power occurring in the frequency range of 0.05 to 0.15 Hz [Vallance Jones, 1974]. A 3 ± 1 Hz modulation of intensity is commonly observed superimposed upon the PA patches [Oliven and Gurnett, 1968; Royrvik and Davis, 1977; Lepine et al., 1980; Sandahl, 1984; Yamamoto, 1988], which will be discussed at length in Section 2.2. The drift speed has been consistently

measured to be on the order of 1 km/s in the morning sector, presumably at the $\mathbf{E} \times \mathbf{B}$ drift speed [Davis, 1978].

A statistical study was done by *Kvifte and Pettersen* [1969] that showed the maximum probability of observing PA was in the equatorward edge of the auroral oval, especially near 0600 MLT. Interestingly, this dawn side sector is the same region in which whistler-mode chorus is seen most prevalently [e.g. *Li et al.*, 2011]. Another statistical study of PA during a solar maximum concluded that there is a 30% probability occurrence of PA near magnetic midnight, which increases dramatically to 100% near 0400 MLT [*Oguti et al.*, 1981].

Jones et al. [2013] presented a case study that detailed the spatial and temporal extent of a long-lasting, widespread PA event. The observations, taken from the array of THEMIS allsky imagers, showed continuous PA lasting approximately 15 hours and covering a maximum span of over 10 hours MLT. The pulsations continued in the easternmost camera until turn-off due to sunlight, implying the pulsations persisted into the daytime sector. This result was just one of several long-lasting events found in 7 months of THEMIS data, suggesting that PA is a common, long-lasting auroral phenomenon that occurs even without a necessary substorm precursor.

Taking the statistical occurrence studies by *Kvifte and Pettersen* [1969] and *Oguti et al.* [1981] together with the case study by *Jones et al.* [2013], it is clear that PA results in a large amount of energy transferred from the magnetosphere to the ionosphere through high energy auroral precipitation. Therefore, the drivers and modulators of PA are important processes to fully understand in order to characterize the magnetosphere-ionosphere coupling interaction.

1.2. Pulsating aurora and chorus

Many previous sounding rocket studies [e.g. *Bryant et al.*, 1975; *Smith et al.*, 1980; *Yau et al.*, 1981; *McEwen et al.*, 1981] have consistently concluded that PA is caused by a few keV to 10's of keV electrons and that the electron populations must originate from geosynchronous orbit, perhaps as a result of scattering by VLF waves. Pitch-angle diffusion via cyclotron resonance interaction is the standard theory for the generation of PA precipitation [*Davidson*, 1986; *Huang et al.*, 1990; *Sandahl*, 1984]. A common scattering theory is outlined by *Kennel and Petschek* [1966] and *Coroniti and Kennel* [1970]. When drifting electrons enter an interaction region, VLF wave growth occurs at the expense of electron perpendicular energy, thereby diffusing those electrons into the loss cone; next, hydromagnetic ULF waves act to modulate the growth of the VLF wave-particle resonance. This flux limiting effect is thought to create periodic strong pitch angle scattering events.

VLF whistler-mode chorus waves are naturally occurring magnetospheric plasma waves observed as wave bursts generated near the magnetic equator [*Burtis and Helliwell*, 1969; *Russell and Holzer*, 1969; *Burtis and Helliwell*, 1976] typically in two distinct frequency bands (upper-band and lower-band), separated by a gap in wave power at half the electron gyrofrequency ($0.5 \Omega_{ce}$). These wave bursts are composed of a discrete superposition of quasi-monochromatic emissions manifest as successions of so-called rising or falling tones [*Sazhin and Hayakawa*, 1992]. It has been shown that chorus amplitudes are dependent on substorm injections, with the largest intensity enhancement seen in the near-midnight to dawn region [*Meredith et al.*, 2001].

A study by *Thorne* [2010] using global statistics from CRRES and Polar, and a numerical model, came to the conclusion that chorus waves are accountable for the scattering of diffuse aurora electrons in the near-midnight and post-midnight sectors. *Nishimura et al.* [2010] provided convincing direct evidence, using THEMIS spacecraft measurements of chorus waves and ground imager observations of PA, that the modulation periods of lower-band chorus waves were closely correlated to PA periods at the footprint of the satellite. A follow-up study that found the same correlations within multiple similar events served as additional evidence that lower-band chorus is indeed the driver of PA [Nishimura et al., 2011]. *Li et al.* [2011] also used THEMIS spacecraft to show a link between lower-band chorus modulations and ground-based observations of PA, in both the temporal and spatial domains. Further evidence of this link was given by *Jaynes et al.* [2013]; this study showed a strong correlation between periodic field-aligned electron fluctuations (at VLF frequencies) seen in the equatorial region using the GOES 13 MagED 30-50 keV and 50-100 keV channels, and PA periods observed with a THEMIS allsky imager at the GOES 13 footprint. The case for pitch-angle scattering by equatorial chorus waves as the driver for PA is a strong one.

1.3. The role of ULF waves

Ultra-low-frequency (ULF) waves in the magnetosphere, spanning frequencies from 1 mHz to 1 Hz, can be characterized as toroidal mode, poloidal mode, or a mixture of the two. (In this paper, we refer to ULF and Pc4-5 interchangeably.) The toroidal mode is exhibited as a magnetic field oscillation in the azimuthal direction, B_ϕ , (with a corresponding radial perturbation in the electric field, E_r) and the poloidal mode is seen as an oscillation in B_r and E_ϕ . The two modes are also associated with different m

numbers, where m denotes the azimuthal wave number from the drift-resonance condition for the drift frequency of a particle at a given energy and drift shell: $\omega_{wave} = m_{wave}\omega_{drift}$ [Southwood *et al.*, 1969]. Low- m ULF waves, corresponding to the toroidal mode, are traditionally thought to occur through coupling from an incoming fast mode wave from the magnetospheric boundary to a standing Alfvén wave mode [e.g. Agapitov *et al.*, 2009]. Higher- m number ULF waves imply a poloidal mode and are thought to arise from particle injections and their subsequent drift motions [e.g. Agapitov and Cherenmykh, 2011].

However, work done on multiple case studies has shown that these two ULF categorizations may not always be generated through separate mechanisms. Many events have been identified where low- to high- m number ULF waves were all generated similarly, through particle injections to the inner magnetosphere [Zolotukhina *et al.*, 2008; Yeoman *et al.*, 2010; James *et al.*, 2013]. The mechanism cited as the cause of these observations invokes the theory detailed in Mager and Klimushkin [2008]. Azimuthally drifting substorm injected ion clouds (in the westward direction) and electron clouds (eastward) comprise the driver for the ULF wave generation. The waves observed in these studies, and explained in the moving-source theory, occur with mixed polarization, at some times being dominantly poloidal and toroidal at others. We therefore see that there can be a causal link between substorm injections and poloidal/toroidal ULF waves.

Additional studies have linked ULF modulations with quasi-periodic chorus wave bursts. Using THEMIS observations, Li *et al.* [2011a] found that Pc4-5 ULF waves can modulate whistler-mode chorus waves, by either changing the electron density or the anisotropy of resonant electrons, thereby affecting the chorus wave growth. Pc4-5 waves occur with periods of tens of seconds to a few minutes, which overlaps precisely with the pulsation

period of typical PA. The implications that this association has for PA generation was explored further in a subsequent paper [*Li et al.*, 2011b] which found that density variations (whether by ULF modulations or otherwise) may be very important in driving PA. Here we can conclude that ULF waves can be substorm generated, may then propagate eastward with the injected electron clouds, and have been seen to affect the periodicity of chorus waves in the inner magnetosphere. Additionally, *Spanswick et al.* [2005] demonstrated that a link exists between precipitation of electrons in the PA energy range and ULF wave periodicities, and furthermore concluded that field line resonances are more efficient at modulating the electron precipitation. Clearly, it is possible for ULF waves to play a role in PA, though the extent of that role has yet to be quantified.

2. Observations: 26 January 2013

For a full examination of this event, we bring together ground-based data from the THEMIS allsky imager array [*Donovan et al.*, 2006] and MOOSE (Multi-spectral Observatory Of Sensitive EMCCDs) imager [see *Michell et al.*, 2014], in-situ wave and particle data from the Van Allen Probes satellites [*Mauk et al.*, 2012], and contextual data of solar wind and geomagnetic indices from OMNI Web. The instrumentation used from the Van Allen Probes includes the EMFISIS (Electric and Magnetic Field Instrument Suite and Integrated Science) fields experiment [*Kletzing et al.*, 2013], the EFW (Electric Field and Waves) fields experiment [*Wygant et al.*, 2013], and the MagEIS (Magnetic Electron Ion Spectrometer) particle detector [*Blake et al.*, 2013] from the ECT (Energetic particle, Composition, and Thermal plasma) instrument suite [*Spence et al.*, 2013].

Beginning on 25 January 2013, a high speed stream solar wind event impacted the magnetosphere, triggering a small geomagnetic storm with minimum Dst reaching ap-

proximately -51 nT. Figure 1 depicts the solar wind and geomagnetic conditions from 25 January 1200 UT through the end of 26 January. The yellow stripe highlights the specific period of interest for this study, during which time correlated ULF and chorus waves were observed in space (discussed in Section 2.1). Intervals of enhanced substorm activity occurred on either side of the period of interest, apparent in the magnitude of the AE index, with activity being somewhat subdued during the event itself. Nevertheless, multiple substorm injections were observed by MagEIS during this time while the Van Allen Probes apogee is located in the post-midnight sector. Figure 2 shows the location of both Van Allen Probes in GSE coordinates (2a), and the footprints of the spacecraft mapped to the ground using the TS04 dynamic magnetic field model [Tsyganenko and Sitnov, 2005] in both geodetic (2b) and magnetic (2c) coordinates over the relevant time period.

Throughout the near-midnight to dawn MLT sector on 26 January 2013, PA was observed in the THEMIS allsky imagers at the Poker Flat, Gillam and The Pas station locations. Figure 3a shows one frame of the Poker Flat allsky imager data at ~1200 UT (0100 MLT). The outlined portion of the image encircles the PA observations; in the zenith direction and extending towards the north, the end of a substorm breakup is visible. The location of the Poker Flat allsky imager is 65.1°N, 212.5°E in geographic coordinates and 65.4°N, 265.9°E in magnetic coordinates. One frame at the same point in time from a mosaic of the full THEMIS array is also shown (Figure 3b), with the Van Allen Probes footprints marked as blue (spacecraft A) and green (spacecraft B) dots. Van Allen Probe-A is on a field line over an imager with no data, and Van Allen Probe-B is located over Whitehorse, which is obscured by cloud cover at this time. However, the

magnetic latitudes (MLAT) of both spacecraft are within 1° of the southern-most portion of the Poker allsky field-of-view (with south being towards the top of Figure 3a), and PA is observed at stations to both the east (Gillam) and west (Poker) of the satellite footprints. Gillam station is located near 333°E magnetic longitude (MLON) and Poker Flat is located near 213°E MLON, while the footprints of the Van Allen Probes are located between 280°E and 315°E MLON during this event. PA is clearly occurring on either side of the Van Allen Probes' footprint and within 15°E MLON during a portion of this time. Since widespread, persistent PA is a common phenomena [Jones *et al.*, 2013], this strongly suggests that PA is very likely occurring directly at the magnetic footprints of the Van Allen Probes, and they are sampling the source region of the precipitation in-situ.

An analysis of the PA event was performed on the Kiana allsky imager (Figure 4), which showed PA in the center view of the imager during the same magnetic local time as PA was seen at Poker, but in a later time UT due to the difference in longitude. Kiana station is located at 65.0°N , 251.5°E in magnetic coordinates. Figure 4 shows a keogram from Kiana that is produced by plotting consecutive north-to-south meridian slices of allsky luminosity in a time series from 1230-1500 UT. There are larger-scale pulsations at Pc4 and Pc5 timescales which are not easily seen in the keogram. However, fast PA is apparent (circled in orange). The observations are aliased due to the 3-second sampling of the imager; therefore, the fast pulsations seen are characterized by 3-second or less periods. Unfortunately, the orbit of Van Allen Probes is at low latitude, heading towards perigee at this time, so a direct comparison of the ground frequencies and in-situ waves is not possible.

Over the course of the Poker Flat allsky movie for the interval surrounding magnetic midnight, three separate substorms are apparent. Utilizing the electron flux data from the MagEIS LOW detector, we can observe the same three substorms in the equatorial region. They are seen as sharp increases in flux across multiple energy channels in Figure 5, which covers approximately two orbits of MagEIS LOW data over energies of 37 keV (highest fluxes) to 221 keV (lowest fluxes). Perigee is seen as dropouts in flux at the start of the plot and near 1600 UT. The first two substorm injections (marked as 1 and 2) cover a wide range of energies, while the third (3) is only clearly seen in the 37 and 57 keV channels. All three show energy dispersion, indicating that the injection site is not co-located with the spacecraft during any of these substorms.

At both spacecraft, coherent oscillations in the magnetic and electric fields are observed with a roughly 2-minute period beginning around the third substorm at ~ 1200 UT. Also clear in the full orbit of EMFISIS waveform data (Figure 6) is an intensification in the lower-band chorus intensity after this same substorm injection. The enhancement is particularly notable in spacecraft B, which saw only sporadic low-level chorus activity for brief period prior to ~ 1200 UT. At shorter time scales, as will be discussed in the next section, the chorus at this time is revealed to be quasi-periodic with a particular modulation frequency.

Figure 7 shows ground magnetometer data from a range of stations across the Alaskan magnetometer chain at similar longitudes. The stations are separated in decreasing MLAT, where the top trace is at the highest MLAT (farthest north) and the bottom trace is at the lowest MLAT (farthest south). The signals are bandpass filtered for frequencies between 10 and 20 mHz. There are indications of a field line resonance [see *Zhu*

and Kivelson, 1989, and references therein] apparent in the magnetometer data: (1) the amplitudes of the wave are typically highest at Poker during this time, and decrease in amplitude at both higher and lower MLAT, and (2) the phase of the wave changes by 180° near a latitudinal point at or below Poker, sometimes seen occurring at the transition between Poker and Gakona, indicating that the resonance occurs between $\sim 65^\circ$ and $\sim 63^\circ$ MLAT.

2.1. Correlation of chorus and ULF

A remarkable feature of the in-situ wave observations is the correlation that exists between the ULF and chorus wave periods (Figures 8 and 9). To directly compare the toroidal and poloidal components of the ULF wave (most strongly observed in the electric field), it was necessary to convert from spacecraft coordinates into the respective contribution to both the radial and azimuthal components. Since the spacecraft spin axis of the Van Allen Probes points in the sunward direction, the axial electric field measurement (mostly aligned with E_X in the mGSE coordinate system) is highly unreliable due to one boom being shadowed by the satellite for much of the time. To obtain the contributions of the axial field to the radial and azimuthal components, we went through the following process using spin-fit electric field data in modified GSE (mGSE) coordinates with a cadence of one sample every twelve seconds. In the mGSE coordinate system, E_X points along the spacecraft spin axis, while E_Y and E_Z are similar to Y and Z GSE (see Wygant *et al.* [2013] for details regarding mGSE). We utilized the Roederer L^* parameter from the Van Allen Probes ephemeris data computed using the TS04 dynamic magnetic field model. Electric field data with $L^* < 2.5$ was removed from consideration because the high velocity of the spacecraft and sharp gradients in the background fields introduced spurious

wave power. We further inspected the electric field data and removed erroneous spikes
 and dropouts in E_y and E_z measurements. We then used magnetic field measurements
 from the EMFISIS instrument suite, at four second resolution in GSE coordinates, and
 rotated them to mGSE coordinates. Assuming orthogonality of the electric and mag-
 netic fields ($E \cdot B = 0$), we derived E_x . Upon division by B_x , the uncertainties in E_x are
 magnified, especially when the magnitude of B_x is small. To limit the influence of such
 uncertainties, we retained E_x only when the angle between the full magnetic field vector
 and the spacecraft spin plane was greater than ten degrees. The three-component electric
 field vector was rotated from mGSE to GSM coordinates, then transformed to polar co-
 ordinates to obtain radial and the azimuthal components of the electric field and proceed
 with the analysis. There were no thruster firings or spacecraft charging events during the
 time period shown that could have otherwise contaminated the component analysis.

Figures 8 and 9 exhibit the correlated modulations in the lower-band chorus and ULF
 wave that exist on both Van Allen Probes spacecraft. The figures are plotted in the
 following identical format first for spacecraft A, then for B: (a) is the wave spectrogram of
 the lower-band chorus in the frequency band of 1-10 kHz, (b) displays the radial component
 of the ULF wave in the electric field (E_r), (c) displays the azimuthal component of the
 ULF wave (E_ϕ), and (d) is a horizontal cut through the chorus wave spectrogram at a
 frequency chosen by eye to represent the peak power spectral density of the modulated
 chorus waves. The poloidal mode oscillations in E_ϕ are observed only on spacecraft A,
 indicating that spacecraft B was sitting at the node of the standing wave. For this time
 period, spacecraft A was closer to the magnetic equator ($MLAT \sim -1^\circ$) while B was near
 -6° MLAT. The striking coherence between the ULF wave periods and the chorus wave

burst periods is clear in both spacecraft for the selected times shown. Interestingly, the chorus modulations appear at ~ 45 second to 1 minute periods, while the ULF periods are closer to 2 minutes, revealing that the ULF waves occur with twice the periodicity as the chorus. The previous study that showed a direct relationship between in-situ ULF and chorus wave periods found a one-to-one variation in the ULF and chorus modulations [Li *et al.*, 2011a].

2.2. Fine structure of chorus

One unexpected component revealed in this event was observed using the burst mode waveform data from the EMFISIS suite. There were multiple burst captures during the event period on both spacecraft, each lasting for a few seconds and exhibiting individual rising tones in the chorus frequency band. These rising tones appear more or less coherent depending on the time period that they are examined, though most of the tones examined occurred at a roughly 3-4 Hz intervals. Figure 10 displays three different burst captures from spacecraft A, the first two panels of which overlap with the time segment of the chorus wave spectrogram in Figure 8. The tones occur at a few-Hz frequency throughout each burst interval (in each of the three panels). Again, this is during a time when PA is occurring in the southern-most portion of the Poker Flat allsky imager, and is likely occurring at the footprint of the Van Allen Probes satellites.

Later in time, around 1500 UT, PA filled the allsky imager at Poker Flat, while Van Allen Probes was simultaneously heading into perigee. However, the MOOSE imager, located at Poker Flat, was recording ground-based optical images at 5577 nm of a narrow field-of-view (5 km x 5 km) at magnetic zenith during this time. The framerate is 44 Hz, ensuring that observations of any high-frequency components of PA at the few-Hz range

are easily resolved. The frequency-time spectrogram taken of the PA observations from 1500-1600 UT is shown in Figure 11. There are many bands that extend through a few-Hz in frequency, with power at times seen up to 10 Hz. Largely, though, the power is confined to 4 Hz or less. This is the same frequency range at which individual rising tones of chorus are observed to occur, albeit at a different point in time (approximately 3 hours earlier). This connection will be discussed in the next section.

3. Discussion and conclusions

In this paper, we present a complete end-to-end observation of a substorm injection driving ULF excitation in both the toroidal and poloidal modes, which then modulates VLF chorus, thus causing periodic pulsating auroral precipitation. A PA event was observed with the THEMIS all-sky imager stationed at Poker Flat, Alaska on 26 January, 2013 from approximately 0035 MLT and persisting to later than 0630 MLT (1730 UT) when the imager was forced to shut off due to sunlight. In-situ observations of the ULF and quasi-periodic chorus waves in the equatorial magnetosphere, using the EMFISIS and EFW wave instrumentation onboard the Van Allen Probes satellites, show a striking correlation in the modulation frequency. The periodicity of the ULF waves is twice that of the chorus, presenting an interesting observation that solicits theoretical study. Periodic density variations caused by the ULF are likely responsible for the VLF growth, as has been suggested by previous studies [e.g. *Li et al.*, 2011b].

A substorm injection was observed in the MagEIS particle detector on the Van Allen Probes just prior to the ULF observations. Analysis of the radial and azimuthal components of the electric field reveal that the ULF wave was a mixture of toroidal and poloidal modes. Such poloidal mode ULF waves are thought to be generated on the tailward

side of the magnetosphere due to energetic particle injections from substorms, specifically westward drifting ion populations *Mager and Klimushkin* [2008]. Recent studies show that some low- m number toroidal ULF waves may also be generated in this fashion [e.g. *James et al.*, 2013].

The substorm injection that occurred near 1200 UT, just prior to the ULF and chorus excitation, also enhanced a region of PA in the equatorward portion of the Poker Flat allsky imager. The TS04 mapped magnetic footprints of the Van Allen Probes were not quite at low enough latitude to fall within the Poker field-of-view, and the all-sky imager that did contain the mapped footprint locations (Whitehorse) was obscured by cloud cover. However, the satellite footprint locations were within 1 degree south and 15 degrees east magnetic latitude of Poker, suggesting that the PA was present at the nearby Van Allen Probes' footprints as well. The frequencies of the chorus wave bursts fall in line with the nearby observed PA modulation frequency. The link has been well established between PA precipitation and VLF chorus in the equatorial region [*Nishimura et al.*, 2011]. Here, we follow that causality back further to link the chorus periods with ULF modulation (of local electron density or resonant electron anisotropies), and even further back to substorm injected electrons.

An intriguing discovery in this data is the observation of a few-Hz frequency seen in the chorus rising tone elements on Van Allen Probes at a time when PA is co-located in the vicinity of the satellite footprint. A superimposed high-frequency component of PA has been reported on for many years in high-framerate optical data [e.g. *Berkey*, 1980], as well as in early sounding rocket experiments [e.g. *Lepine et al.*, 1980]. In addition to the oft-observed 3-Hz frequency, *Kataoka et al.* [2012] found pulsations embedded in PA at

frequencies up to 50 Hz, although the dominant power was contained in somewhat lower frequencies. The authors speculate that a 3 ± 1 Hz frequency emanating from chorus in the equatorial region is well defined, though the higher frequencies may have a source in the magnetosphere-ionosphere coupling region. Our observations are consistent with this proposition: chorus elements observed in space show the 3 ± 1 Hz frequency, while the high-speed ground imager shows a range of higher frequencies at times, though mainly confined to near the few-Hz regime. The mechanism for the chorus elements acting to produce the high-frequency pulsations is a nonlinear interaction resulting in strong pitch angle scattering, as is very well explained in *Nishiyama et al.* [2014].

The case study presented here follows a substorm injection, a generated Pc4-5 ULF wave observed as a field line resonance, a correlated VLF chorus wave occurring at half the periodicity of the ULF wave, and ground observations of PA. We demonstrate the direct connection between this string of events, many components of which have been implied by previous studies. Further study is needed to test whether this sequence is the dominant driver of pulsating aurora, but this will require an extensive statistical database which is not attainable with the limited conjunctive measurements available at present. Even more specifically, the link between ULF modulations and whistler-mode chorus periods warrants greater attention, since this has implications beyond that of PA. More theoretical and observational analysis needs to be performed to investigate the physics involved in the ULF and quasi-periodic chorus periodicity correlation. Nevertheless, the emerging picture of substorm-driven ULF modulating the chorus which ends up as the driver of PA is one that deserves notice.

Acknowledgments. This work was primarily performed with RBSP-ECT funding through JHU/APL contract 428 967399 (under prime NASA contract NAS5-01072) and NASA grant NNX13AO43H. Work at JHUAPL was supported by NASA grant NNX14AB97G. Work by R. G. M. was supported by NSF grants: AGS-1456161 and AGS-1456129. All Van Allen Probes data presented here is publicly available via CDAweb or the individual instrument team websites. ACE/WIND solar wind data and various geomagnetic indices are available through CDAweb as well. Ground magnetometer data was obtained through the University of Alaska Geophysical Institute magnetometer array and associated web data directory. The Kiana THEMIS system is operated by UC Berkeley supported by NSF. We wish to thank Brian Jackel for his contributions to this study.

References

- Agapitov, A. V., and O. K. Cheremnykh (2011), Polarization of ULF waves in the earth's magnetosphere, *Kinematics and Physics of Celestial Bodies*, *27*, 117–123.
- Agapitov, O., K.-H. Glassmeier, F. Plaschke, H.-U. Auster, D. Constantinescu, V. Angelopoulos, W. Magnes, R. Nakamura, C. W. Carlson, S. Frey, and J. P. McFadden (2009), Surface waves and field line resonances: A THEMIS case study, *Journal of Geophysical Research (Space Physics)*, *114*, A00C27, doi:10.1029/2008JA013553.
- Berkey, F. T. (1980), Temporal fluctuations in the luminosity of diffuse aurora, *J. Geophys. Res.*, *85*(A11), 6075–6079, doi:10.1029/JA085iA11p06075.
- Blake, J. B., P. A. Carranza, S. G. Claudepierre, J. H. Clemmons, W. R. Crain, Y. Dotan, J. F. Fennell, F. H. Fuentes, R. M. Galvan, J. S. George, M. G. Henderson, M. Lalic, A. Y. Lin, M. D. Looper, D. J. Mabry, J. E. Mazur, B. McCarthy, C. Q. Nguyen,

380 T. P. O'Brien, M. A. Perez, M. T. Redding, J. L. Roeder, D. J. Salvaggio, G. A.
381 Sorensen, H. E. Spence, S. Yi, and M. P. Zakrzewski (2013), The Magnetic Electron Ion
382 Spectrometer (MagEIS) Instruments Aboard the Radiation Belt Storm Probes (RBSP)
383 Spacecraft, *Space Science Reviews*, doi:10.1007/s11214-013-9991-8.

384 Bryant, D., M. Smith, and G. Courtier (1975), Distant modulation of electron intensity
385 during the expansion phase of an auroral substorm, *Planetary and Space Science*, *23*(5),
386 867–878, doi:10.1016/0032-0633(75)90022-7.

387 Burtis, W. J., and R. A. Helliwell (1969), Banded Chorus - A New Type of VLF Radiation
388 Observed in the Magnetosphere by OGO 1 and OGO 3, *J. Geophys. Res.*, *74*(11), 3002–
389 3010, doi:10.1029/JA074i011p03002.

390 Burtis, W. J., and R. A. Helliwell (1976), Magnetospheric chorus: Occurrence patterns and
391 normalized frequency, *Planetary and Space Science*, *24*, 1007–1024, doi:10.1016/0032-
392 0633(76)90119-7.

393 Coroniti, F., and C. Kennel (1970), Auroral micropulsation instability, *J. Geophys. Res.*,
394 *75*(10), 1863–1878.

395 Davidson, G. (1986), Pitch Angle Diffusion in Morningside Aurorae, 1. The Role of the
396 Loss Cone in the Formation of Impulsive Bursts of Precipitation, *J. Geophys. Res.*,
397 *91*(A4), 4413–4427, doi:10.1029/JA091iA04p04413.

398 Davis, T. (1978), Observed characteristics of auroral forms, *Space Science Reviews*, *22*(1),
399 77–113.

400 Donovan, E., S. Mende, B. Jackel, H. Frey, M. T. Syrjasuo, I. Voronkov, T. Trondsen,
401 L. M. Peticolas, V. Angelopoulos, S. Harris, M. Greffen, and M. Connors (2006), The
402 THEMIS all-sky imaging array-system design and initial results from the prototype

imager, *Journal of Atmospheric and Solar-Terrestrial Physics*, 68, 1472–1487.

Duncan, C. N., F. Creutzberg, R. L. Gattinger, F. R. Harris, and A. Vallance Jones (1981), Latitudinal and temporal characteristics of pulsating auroras, *Canadian Journal of Physics*, 59, 1063–1069, doi:10.1139/p81-140.

Huang, L., J. Hawkins, and L. Lee (1990), On the generation of the pulsating aurora by the loss cone driven whistler instability in the equatorial region, *J. Geophys. Res.*, 95(A4), 3893–3906, doi:10.1029/JA095iA04p03893.

James, M. K., T. K. Yeoman, P. N. Mager, and D. Y. Klimushkin (2013), The spatio-temporal characteristics of ULF waves driven by substorm injected particles, *Journal of Geophysical Research (Space Physics)*, 118, 1737–1749, doi:10.1002/jgra.50131.

Jaynes, A. N., M. R. Lessard, J. V. Rodriguez, E. Donovan, T. M. Loto’Aniu, and K. Rychert (2013), Pulsating auroral electron flux modulations in the equatorial magnetosphere, *J. Geophys. Res. Space Physics*, 118(8), 4884–4894, doi:10.1002/jgra.50434.

Johnstone, A. (1978), Pulsating aurora, *Nature*, 274, 119–126, doi:10.1038/274119a0.

Jones, S. L., M. R. Lessard, K. Rychert, E. Spanswick, E. Donovan, and A. N. Jaynes (2013), Persistent, widespread pulsating aurora: A case study, *J. Geophys. Res. Space Physics*, 118(6), 2998–3006, doi:10.1002/jgra.50301.

Kataoka, R., Y. Miyoshi, D. Hampton, T. Ishii, and H. Kozako (2012), Pulsating aurora beyond the ultra-low-frequency range, *J. Geophys. Res.*, 117(A8), A08,336, doi:10.1029/2012JA017987.

Kennel, C. F., and H. E. Petschek (1966), Limit on Stably Trapped Particle Fluxes, *J. Geophys. Res.*, 71(1), 1–&.

Kletzing, C. A., W. S. Kurth, M. Acuna, R. J. MacDowall, R. B. Torbert, T. Averkamp,
D. Bodet, S. R. Bounds, M. Chutter, J. Connerney, D. Crawford, J. S. Dolan,
R. Dvorsky, G. B. Hospodarsky, J. Howard, V. Jordanova, R. A. Johnson, D. L. Kirchner,
B. Mokrzycki, G. Needell, J. Odom, D. Mark, R. Pfaff, J. R. Phillips, C. W.
Piker, S. L. Remington, D. Rowland, O. Santolik, R. Schnurr, D. Sheppard, C. W.
Smith, R. M. Thorne, and J. Tyler (2013), The Electric and Magnetic Field Instrument Suite and Integrated Science (EMFISIS) on RBSP, *Space Sci. Rev.*, *179*, 127–181, doi:10.1007/s11214-013-9993-6.

Kvifte, G. J., and H. Pettersen (1969), Morphology of the pulsating aurora, *Planet. Space Sci.*, *17*, 1599–1607, doi:10.1016/0032-0633(69)90148-2.

Lepine, D., D. Bryant, and D. Hall (1980), A 2.2-Hz modulation of auroral electrons imposed at the geomagnetic equator, *Nature*, *286*, 469–471.

Li, W., J. Bortnik, R. M. Thorne, and V. Angelopoulos (2011), Global distribution of wave amplitudes and wave normal angles of chorus waves using THEMIS wave observations, *J. Geophys. Res.*, *116*(A), 12,205, doi:10.1029/2011JA017035.

Li, W., R. M. Thorne, J. Bortnik, Y. Nishimura, and V. Angelopoulos (2011a), Modulation of whistler mode chorus waves: 1. Role of compressional Pc4-5 pulsations, *Journal of Geophysical Research (Space Physics)*, *116*, A06205, doi:10.1029/2010JA016312.

Li, W., J. Bortnik, R. M. Thorne, Y. Nishimura, V. Angelopoulos, and L. Chen (2011b), Modulation of whistler mode chorus waves: 2. Role of density variations, *Journal of Geophysical Research (Space Physics)*, *116*, A06206, doi:10.1029/2010JA016313.

Mager, P. N., and D. Y. Klimushkin (2008), Alfvén ship waves: high-m ULF pulsations in the magnetosphere generated by a moving plasma inhomogeneity, *Annales Geophysicae*,

26, 1653–1663, doi:10.5194/angeo-26-1653-2008.

Mauk, B. H., N. J. Fox, S. G. Kanekal, R. L. Kessel, D. G. Sibeck, and A. Ukhorskiy (2012), Science Objectives and Rationale for the Radiation Belt Storm Probes Mission, *Space Science Reviews*, 179(1-4), 3–27, doi:10.1007/s11214-012-9908-y.

McEwen, D. J., E. Yee, B. A. Whalen, and A. W. Yau (1981), Electron energy measurements in pulsating auroras, *Canadian Journal of Physics*, 59, 1106–1115, doi:10.1139/p81-146.

Meredith, N. P., R. B. Horne, and R. R. Anderson (2001), Substorm dependence of chorus amplitudes: Implications for the acceleration of electrons to relativistic energies, *J. Geophys. Res.*, , 106, 13,165–13,178, doi:10.1029/2000JA900156.

Michell, R. G., T. Grydeland, and M. Samara (2014), Characteristics of Poker Flat Incoherent Scatter Radar (PFISR) naturally enhanced ion-acoustic lines (NEIALs) in relation to auroral forms, *Annales Geophysicae*, 32, 1333–1347, doi:10.5194/angeo-32-1333-2014.

Nishimura, Y., L. R. Lyons, S. Zou, X. Xing, V. Angelopoulos, S. B. Mende, J. W. Bonnell, D. Larson, U. Auster, T. Hori, N. Nishitani, K. Hosokawa, G. Sofko, M. Nicolls, and C. Heinselman (2010), Preonset time sequence of auroral substorms: Coordinated observations by all-sky imagers, satellites, and radars, *J. Geophys. Res.*, 115, A00I08, doi:10.1029/2010JA015832.

Nishimura, Y., J. Bortnik, W. Li, R. M. Thorne, L. Chen, L. R. Lyons, V. Angelopoulos, S. B. Mende, J. Bonnell, O. Le Contel, C. Cully, R. Ergun, and U. Auster (2011), Multievent study of the correlation between pulsating aurora and whistler mode chorus emissions, *J. Geophys. Res.*, 116(A11), A11,221, doi:10.1029/2011JA016876.

- Nishiyama, T., T. Sakanoi, Y. Miyoshi, D. L. Hampton, Y. Katoh, R. Kataoka, and S. Okano (2014), Multiscale temporal variations of pulsating auroras: On-off pulsation and a few Hz modulation, *J. Geophys. Res. Space Physics*, *119*(5), 3514–3527, doi:10.1002/2014JA019818.
- Oguti, T., S. Kokubun, K. Hayashi, K. Tsuruda, S. Machida, T. Kitamura, O. Saka, and T. Watanabe (1981), Statistics of pulsating auroras on the basis of all-sky TV data from five stations. I - Occurrence frequency, *Canadian Journal of Physics*, *59*, 1150–1157, doi:10.1139/p81-152.
- Oliven, M. N., and D. A. Gurnett (1968), Microburst phenomena: 3. An association between microbursts and VLF chorus, *J. Geophys. Res.*, *73*(7), 2355–2362, doi:10.1029/JA073i007p02355.
- Omholt, A. (1971), *The optical aurora*.
- Royrvik, O., and T. Davis (1977), Pulsating aurora: Local and global morphology, *J. Geophys. Res.*, *82*(29), 4720–4740, doi:10.1029/JA082i029p04720.
- Russell, C. T., and R. E. Holzer (1969), OGO 3 observations of ELF noise in the magnetosphere, 1. Spatial extent and frequency of occurrence, *J. Geophys. Res.*, *74*(3), 755–777, doi:10.1029/JA074i003p00755.
- Sandahl, I. (1984), Pitch angle scattering and particle precipitation in a pulsating aurora: An experimental study, *Tech. rep.*
- Sazhin, S., and M. Hayakawa (1992), Magnetospheric chorus emissions: A review, *Planetary and Space Science*, *40*(5), 681–697, doi:10.1016/0032-0633(92)90009-D.
- Smith, M. J., D. A. Bryant, and T. Edwards (1980), Pulsations in auroral electrons and positive ions, *Journal of Atmospheric and Terrestrial Physics*, *42*, 167–178.

Southwood, D. J., J. W. Dungey, and R. J. Etherington (1969), Bounce resonant interaction between pulsations and trapped particles, *Planetary Sp. Sci.*, *17*, 349–361, doi:10.1016/0032-0633(69)90068-3.

Spanswick, E., E. Donovan, and G. Baker (2005), Pc5 modulation of high energy electron precipitation: particle interaction regions and scattering efficiency, *Annales Geophysicae*, *23*, 1533–1542, doi:10.5194/angeo-23-1533-2005.

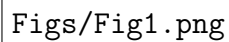
Spence, H. E., G. D. Reeves, D. N. Baker, J. B. Blake, M. Bolton, S. Bourdarie, A. A. Chan, S. G. Claudepierre, J. H. Clemmons, J. P. Cravens, S. R. Elkington, J. F. Fennell, R. H. W. Friedel, H. O. Funsten, J. Goldstein, J. C. Green, A. Guthrie, M. G. Henderson, R. B. Horne, M. K. Hudson, J.-M. Jahn, V. K. Jordanova, S. G. Kanekal, B. W. Klatt, B. A. Larsen, X. Li, E. A. MacDonald, I. R. Mann, J. Niehof, T. P. O’Brien, T. G. Onsager, D. Salvaggio, R. M. Skoug, S. S. Smith, L. L. Suther, M. F. Thomsen, and R. M. Thorne (2013), Science Goals and Overview of the Radiation Belt Storm Probes (RBSP) Energetic Particle, Composition, and Thermal Plasma (ECT) Suite on NASA’s Van Allen Probes Mission, *Space Science Reviews*, *179*, 311–336, doi:10.1007/s11214-013-0007-5.

Thorne, R. M. (2010), Radiation belt dynamics: The importance of wave-particle interactions, *Geophys. Res. Lett.*, *37*(22), L22,107, doi:10.1029/2010GL044990.

Tsyganenko, N. A., and M. I. Sitnov (2005), Modeling the dynamics of the inner magnetosphere during strong geomagnetic storms, *J. Geophys. Res.*, *110*(A03208), doi:10.1029/2004JA010798.

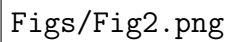
Vallance Jones, A. (1974), *Aurora*.

- Wygant, J. R., J. W. Bonnell, K. Goetz, R. E. Ergun, F. S. Mozer, S. D. Bale, M. Ludlam,
P. Turin, P. R. Harvey, R. Hochmann, K. Harps, G. Dalton, J. McCauley, W. Rachel-
son, D. Gordon, B. Donakowski, C. Shultz, C. Smith, M. Diaz-Aguado, J. Fischer,
S. Heavner, P. Berg, D. M. Malsapina, M. K. Bolton, M. Hudson, R. J. Strangeway,
D. N. Baker, X. Li, J. Albert, J. C. Foster, C. C. Chaston, I. Mann, E. Donovan, C. M.
Cully, C. A. Cattell, V. Krasnoselskikh, K. Kersten, A. Brenneman, and J. B. Tao
(2013), The Electric Field and Waves Instruments on the Radiation Belt Storm Probes
Mission, *Space Sci. Rev.*, *179*, 183–220, doi:10.1007/s11214-013-0013-7.
- Yamamoto, T. (1988), On the temporal fluctuations of pulsating auroral luminosity, *J.*
Geophys. Res., *93*(A2), 897–911, doi:10.1029/JA093iA02p00897.
- Yau, A. W., B. A. Whalen, and d. j. mcewen (1981), Rocket-borne measurements
of particle pulsation in pulsating aurora, *J. Geophys. Res.*, *86*(A7), 5673–5681, doi:
10.1029/JA086iA07p05673.
- Yeoman, T. K., D. Y. Klimushkin, and P. N. Mager (2010), Intermediate-m ULF waves
generated by substorm injection: a case study, *Annales Geophysicae*, *28*, 1499–1509,
doi:10.5194/angeo-28-1499-2010.
- Zhu, X. M., and M. G. Kivelson (1989), Global Mode Ulf Pulsations in a Magnetosphere
with a Nonmonotonic Alfven Velocity Profile, *J. Geophys. Res. Space Physics*, *94*(A2),
1479–1485, doi:10.1029/JA094iA02p01479.
- Zolotukhina, N. A., P. N. Mager, and D. Y. Klimushkin (2008), Pc5 waves gener-
ated by substorm injection: a case study, *Annales Geophysicae*, *26*, 2053–2059, doi:
10.5194/angeo-26-2053-2008.



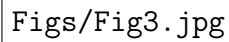
Figs/Fig1.png

Figure 1. Solar wind conditions and geomagnetic indices for 25 Jan 2013, 1200 UT through 26 Jan 2013, showing the effects of a high speed stream impacting the magnetosphere. The highlighted portion indicates the time of wave observations on the Van Allen Probes and ground-based pulsating aurora observations.




Figs/Fig2.png

Figure 2. The positional parameters of the Van Allen Probes, 26 January 2013 1100-1500 UT. (a) GSE location of the spacecraft and Northern hemisphere footprints for (b) magnetic and (c) geodetic coordinates derived using the TS04 magnetic field model.



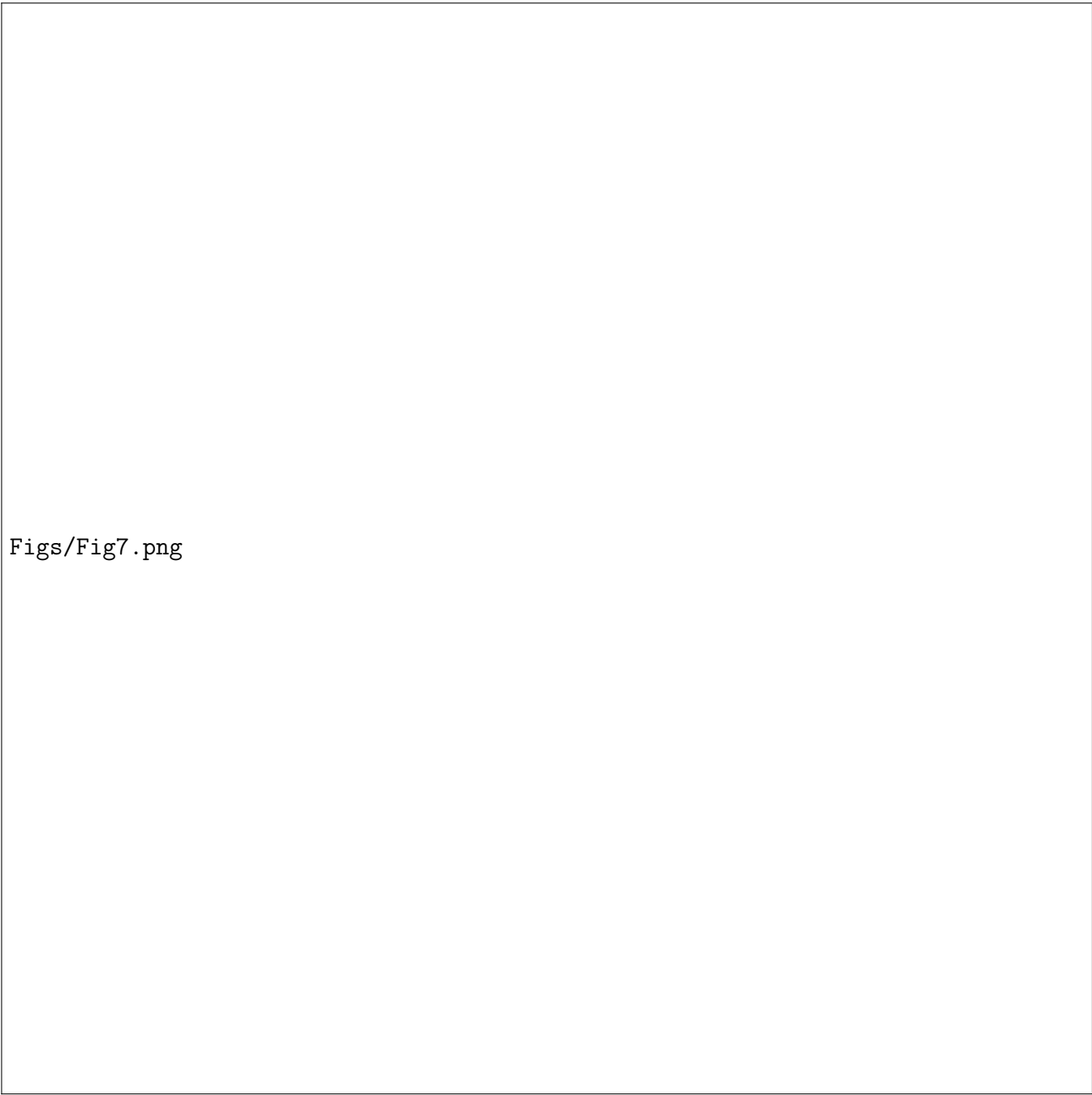
Figs/Fig3.jpg

Figure 3. Pulsating aurora observations from (a) the Poker Flat allsky near the footprint of the Van Allen Probes at ~ 1200 UT and (b) the THEMIS allsky imager array mosaic at the same time with Van Allen Probes footprint shown as green and blue markers.



Figs/kiana.pdf

Figure 4. Keogram from Kiana allsky imager showing relative luminosity in a latitude versus time format with ≤ 3 Hz pulsations circled (top panel) and raw CCD counts along the North-South meridian (bottom panel). The time of 0200 MLT is denoted by the green line.

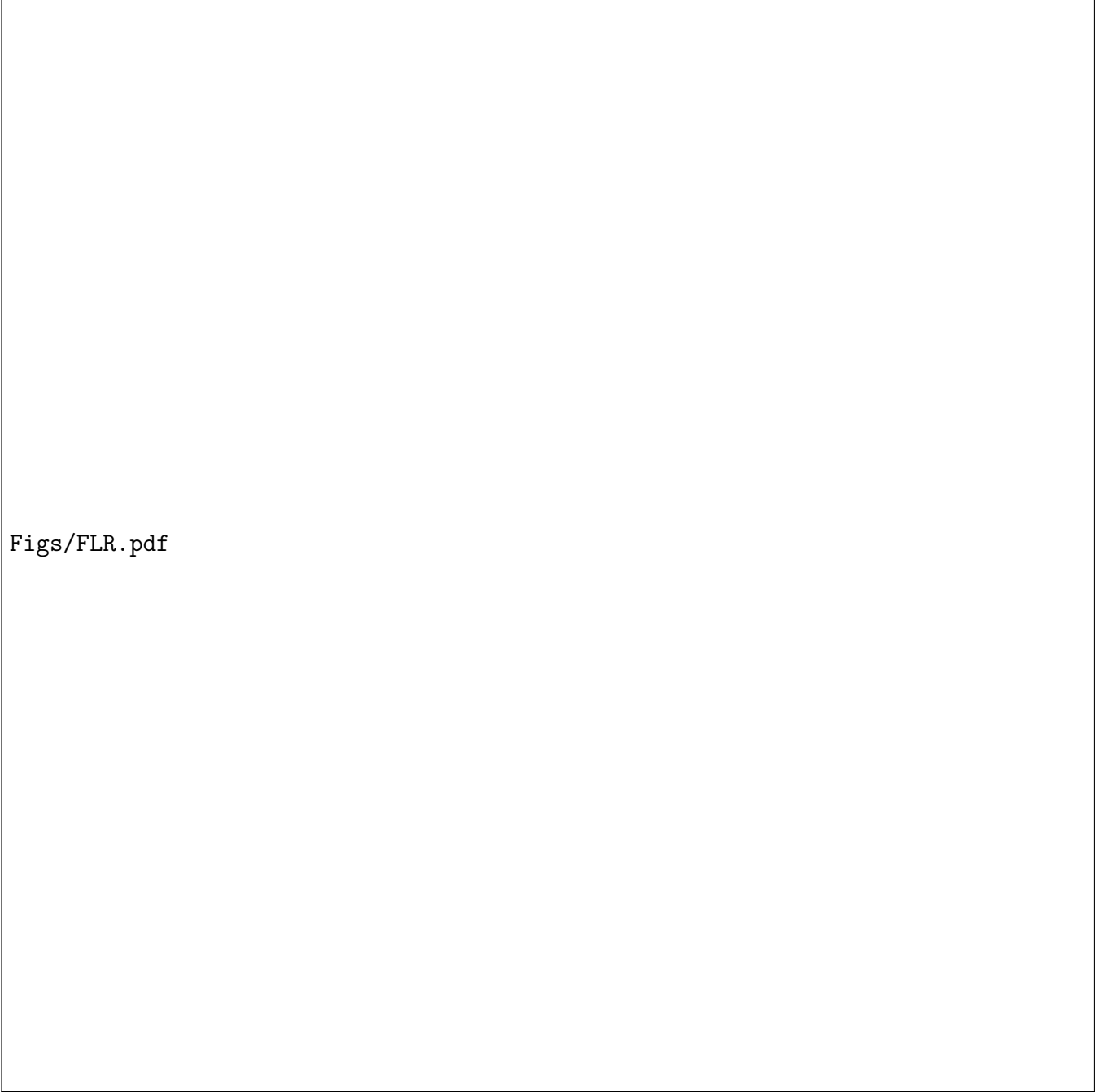


Figs/Fig7.png

Figure 5. Three individual substorm injections (marked 1, 2, 3) observed by MagEIS-A LOW over the orbit covering approximately 0800 to 1600 UT on 26 January 2013. Substorm 3 occurs just prior to the plasma wave oscillations shown in Figures 8 and 9.

Figs/Fig_chorus.pdf

Figure 6. EMFISIS waveform spectra of chorus wave power on Van Allen Probes A and B spacecraft for the full day of 26 January 2013. Dashed lines denote 0.1, 0.5 and 1.0 times the electron gyrofrequency, with upper-band chorus and lower-band chorus separated by the red line at half the electron gyrofrequency.



Figs/FLR.pdf

Figure 7. Ground magnetometer data bandpass filtered for frequencies between 10 and 20 mHz at four stations from the Alaskan magnetometer chain. Stations are plotted in decreasing magnetic latitude from top to bottom.

Figs/Fig4.png

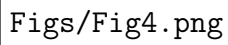
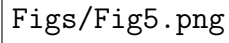
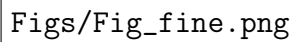


Figure 8. Chorus and ULF waves observed in-situ onboard the Van Allen Probes A spacecraft from 1215 to 1225 UT. (a) Wave spectrogram showing whistler-mode chorus in lower band (lines depict fractions of local electron cyclotron frequency), (b) E_r and (c) E_ϕ electric field components showing ULF wave observations and (d) a line cut through the chorus spectrogram at ~ 890 Hz.



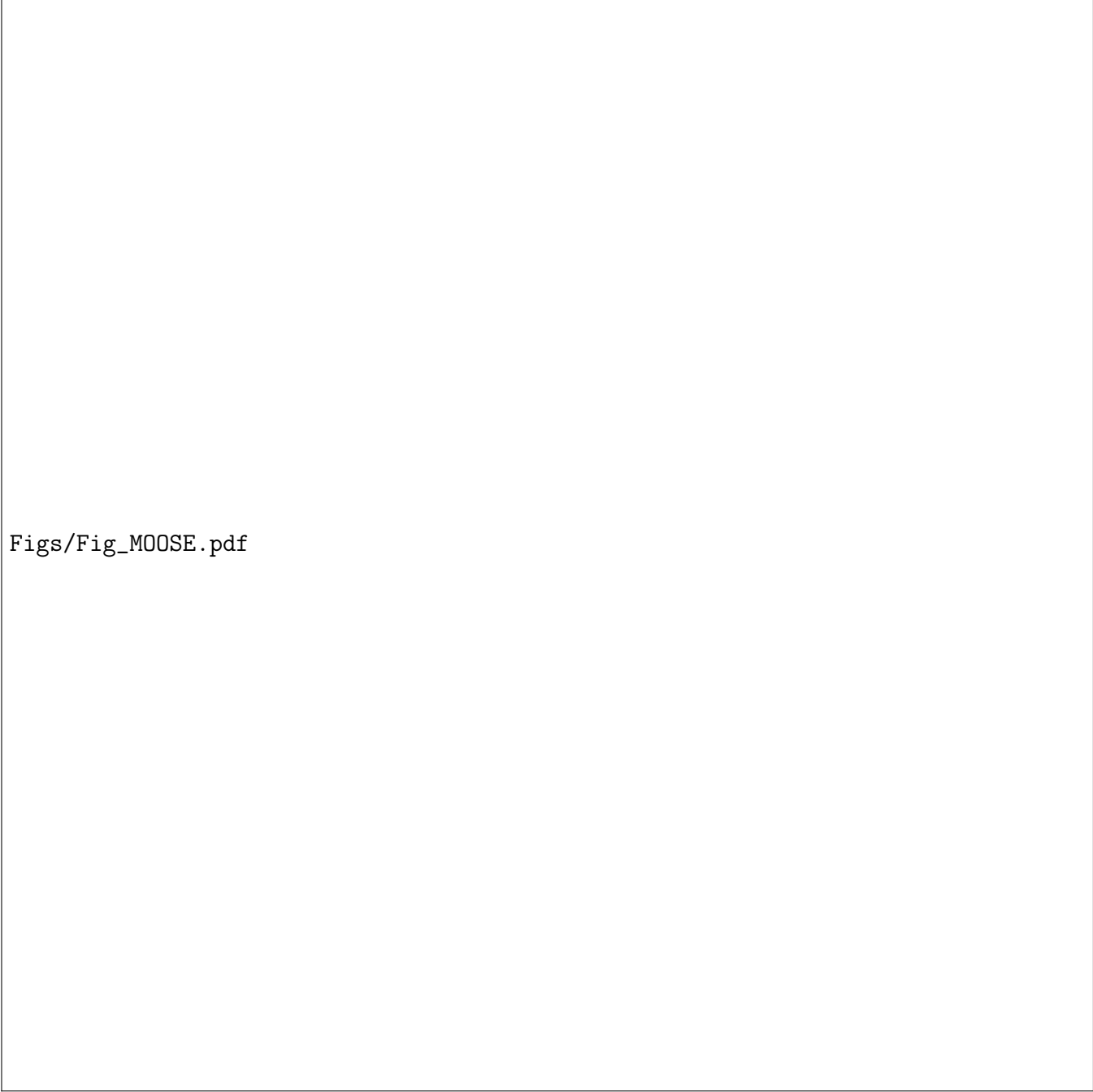
Figs/Fig5.png

Figure 9. Chorus and ULF waves observed in-situ onboard the Van Allen Probes B spacecraft from 1150 to 1200 UT. (a) Wave spectrogram showing whistler-mode chorus in lower band (lines depict fractions of local electron cyclotron frequency), (b) E_r and (c) E_ϕ electric field components showing ULF wave observations and (d) a line cut through the chorus spectrogram at ~ 709 Hz.



Figs/Fig_fine.png

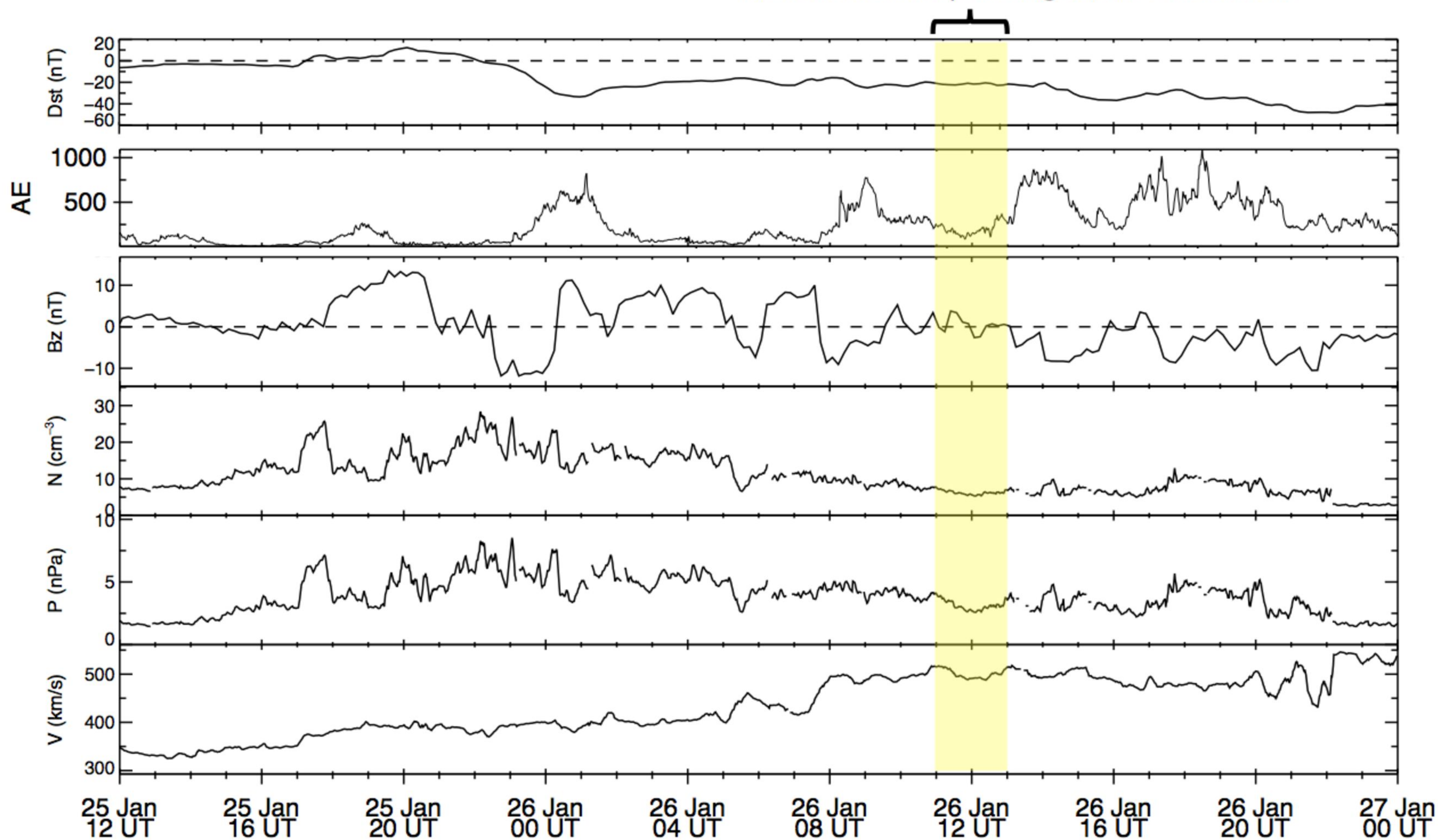
Figure 10. High time resolution EMFISIS burst mode waveform captures of discrete rising tones within several individual lower-band chorus wave bursts observed on spacecraft A. The rising tones occur at a few-Hz frequency.

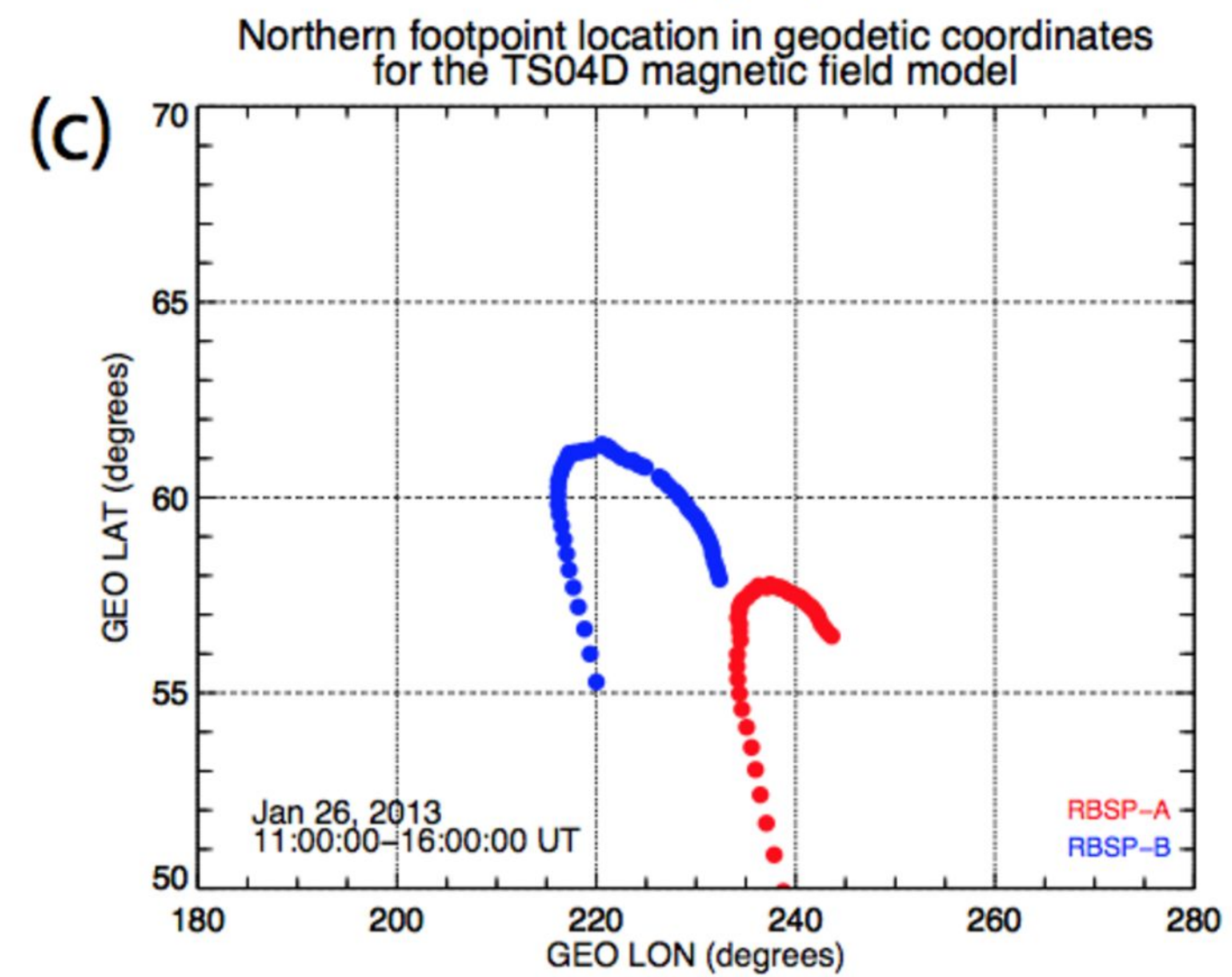
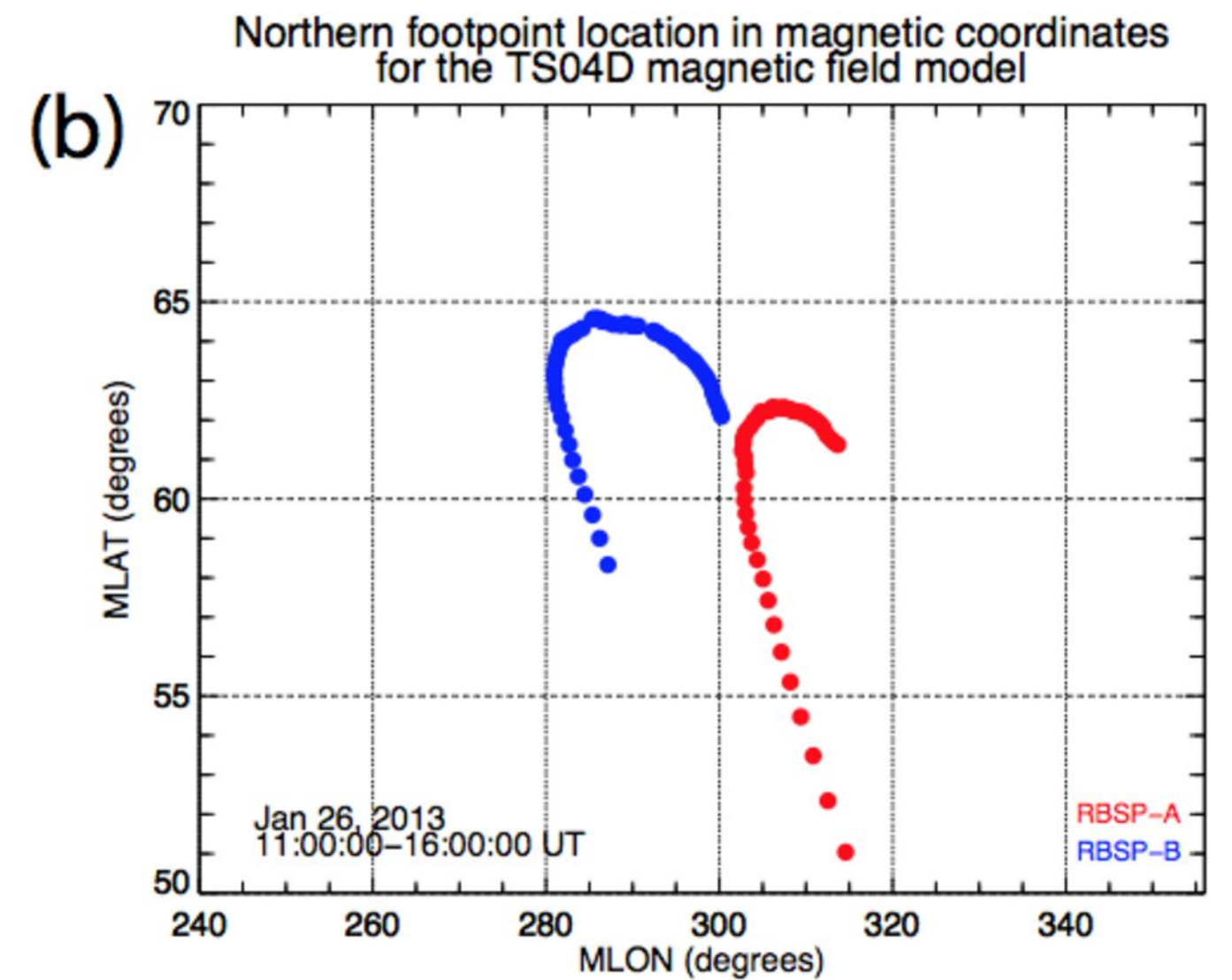
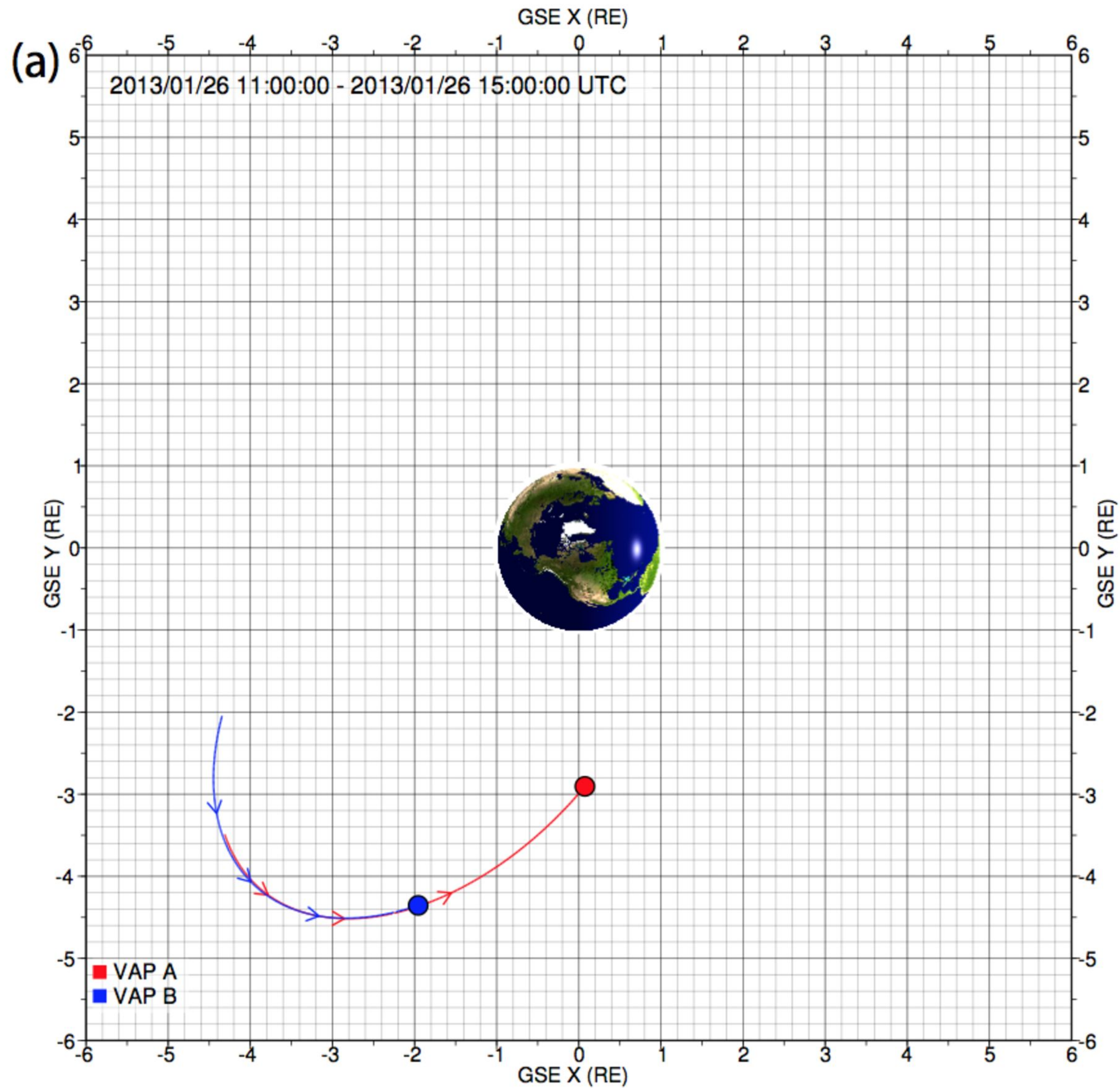


Figs/Fig_MOOSE.pdf

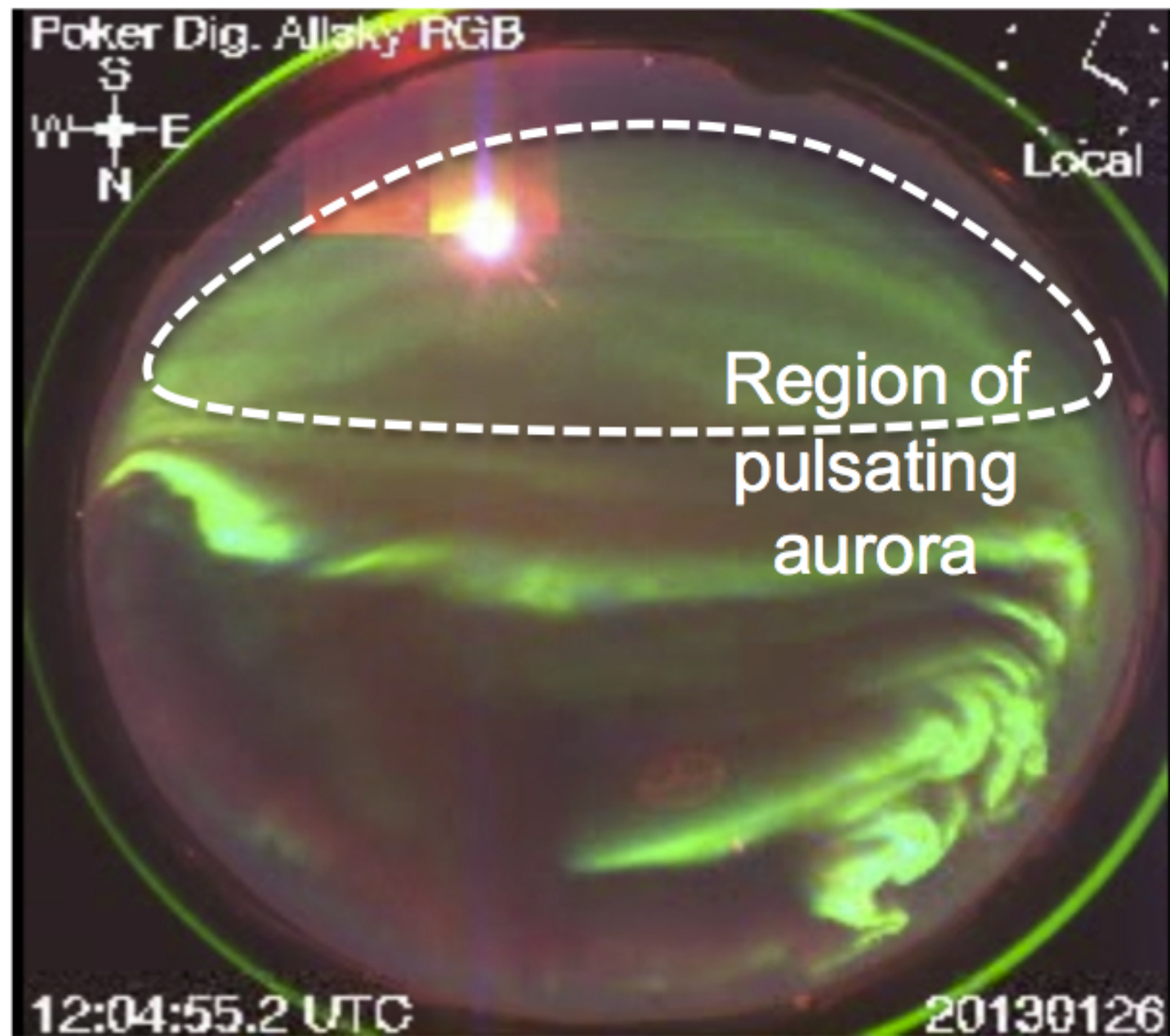
Figure 11. Frequency analysis of the high-framerate MOOSE ground-based imager data from 1500-1600 UT, at a time when PA fills the visible sky at Poker Flat.

In-situ waves and pulsating aurora observations

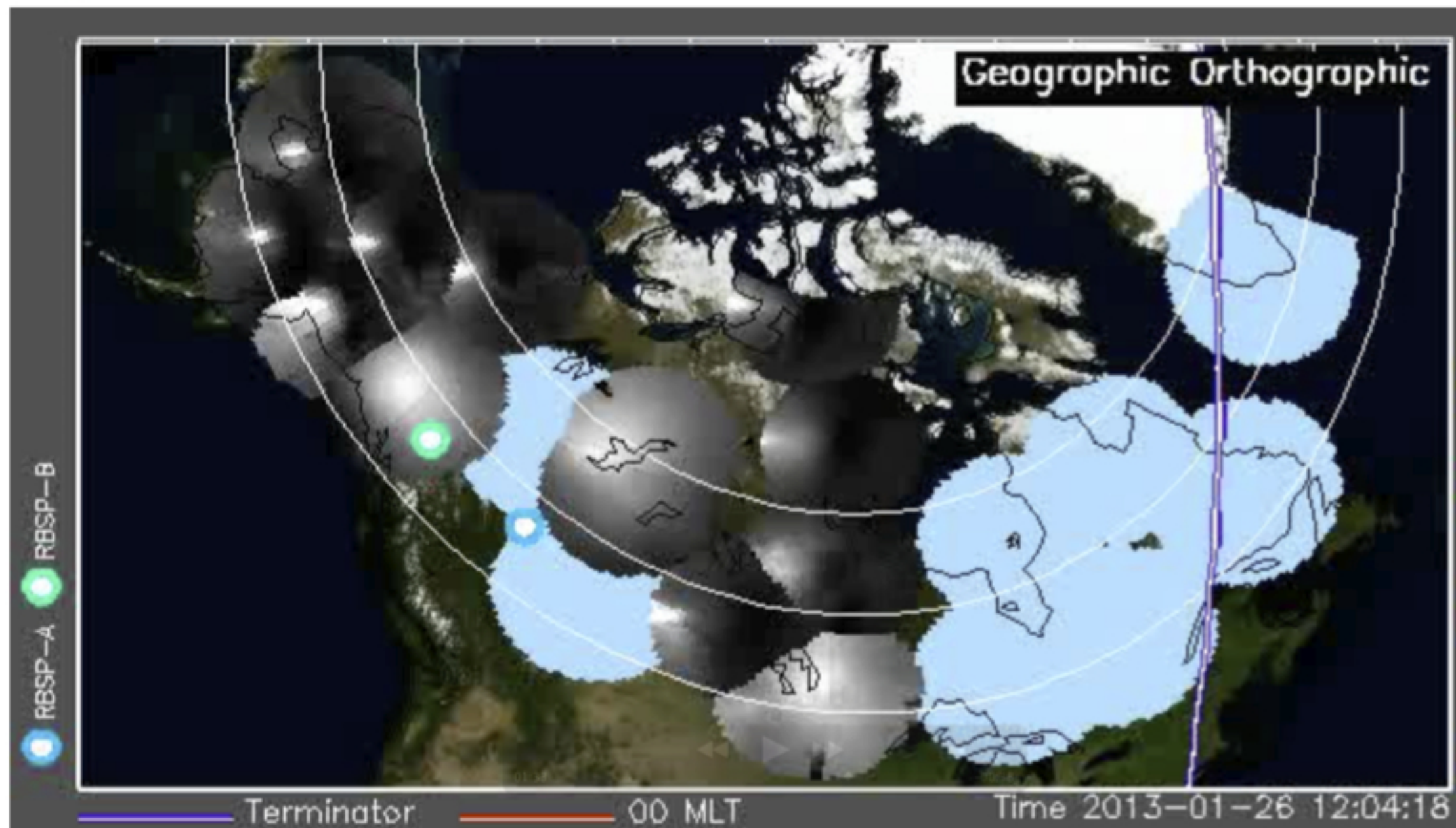


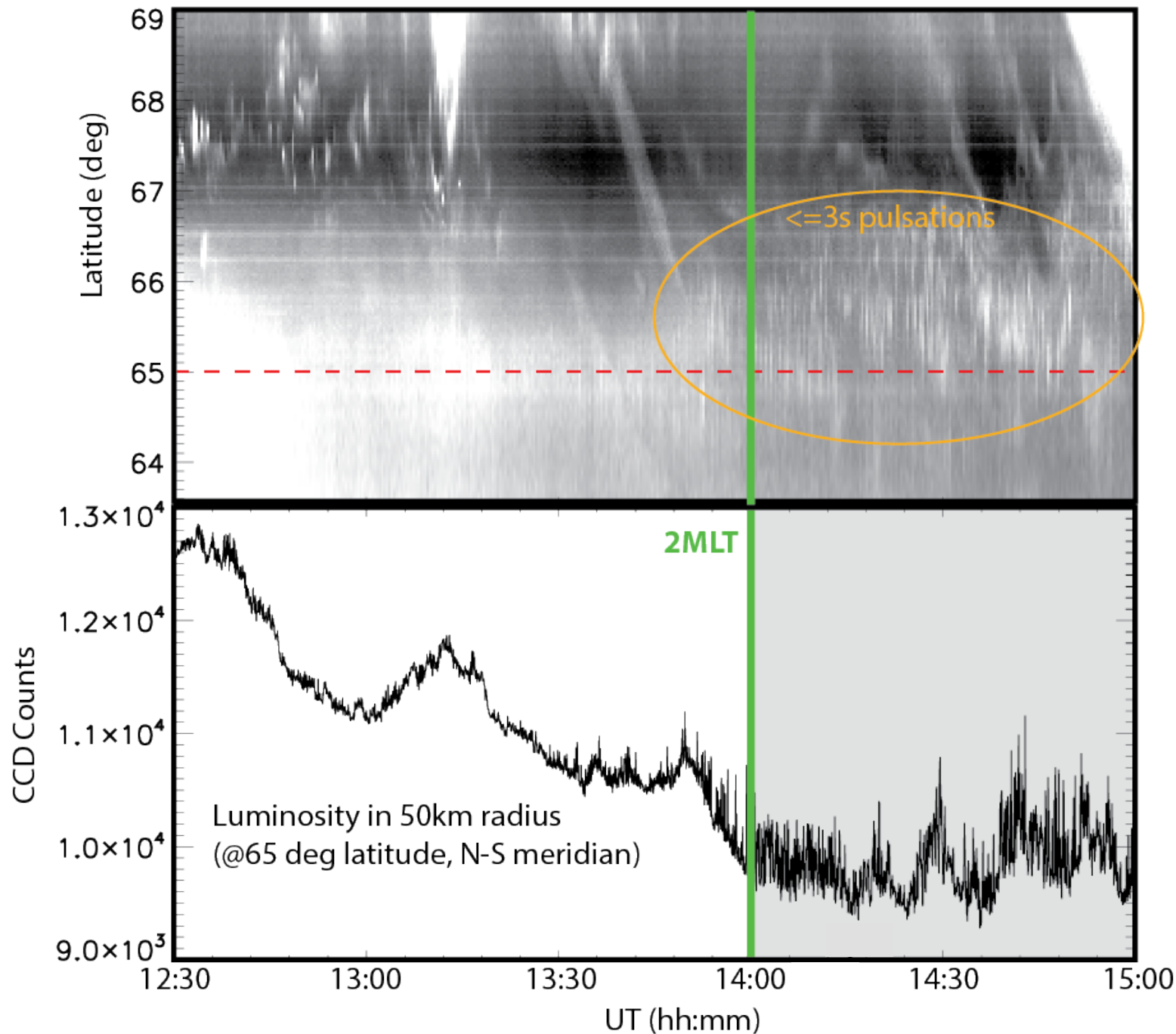


a)

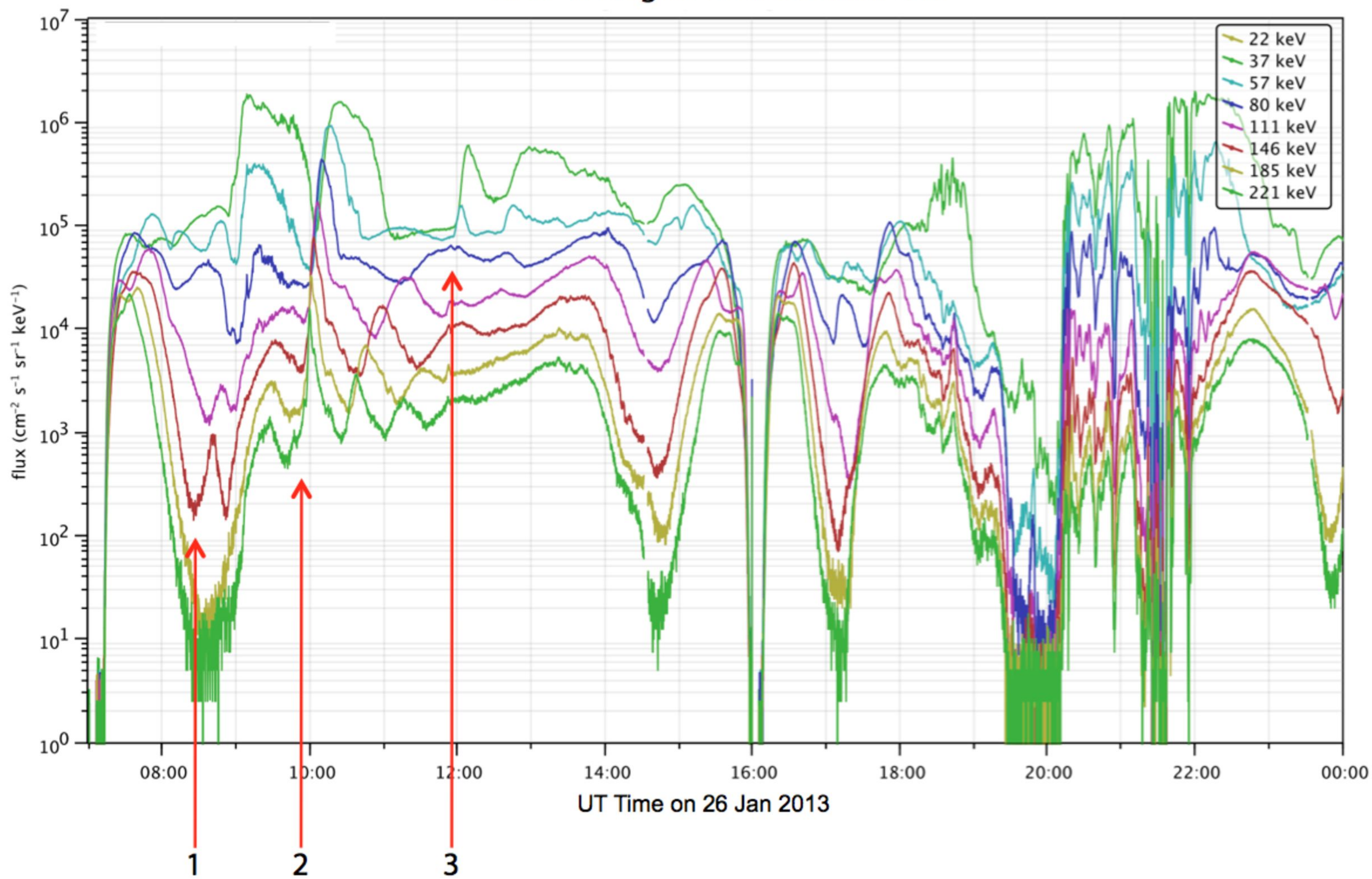


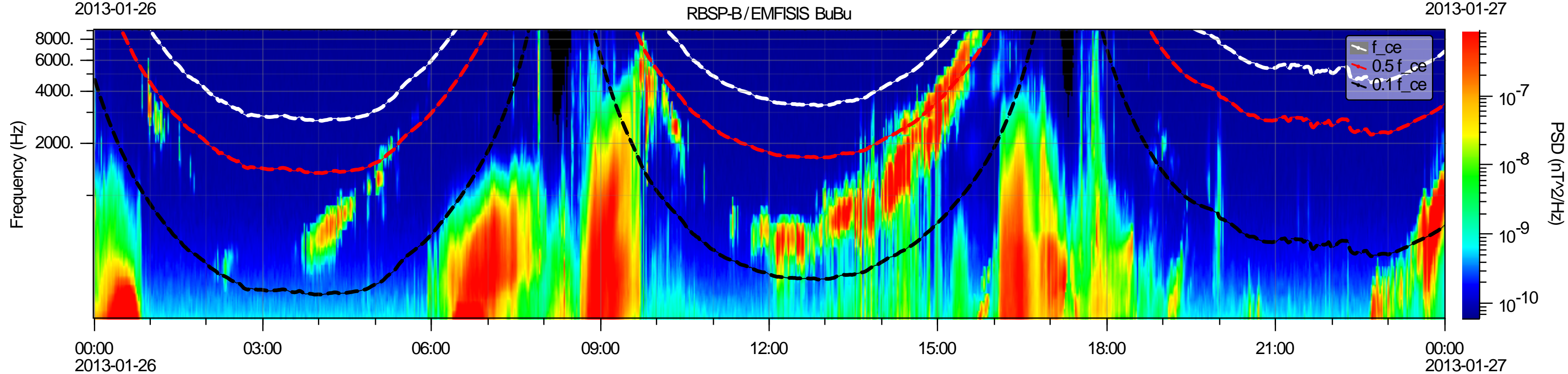
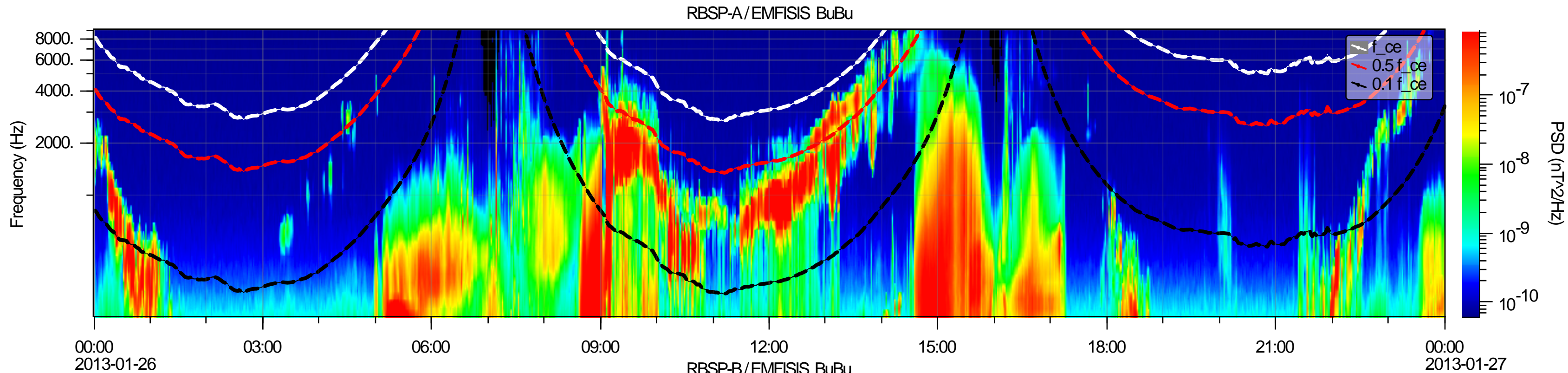
b)





RBSP-A MagEIS LOW electron flux





H-Component

10 mHz < f < 20 mHz

10 nT / division

Kaktovik
71.0 MLAT

Fort Yukon
67.3 MLAT

Poker
65.1 MLAT

Gakona
63.1 MLAT

11:50:00

11:55:00

12:00:00

12:05:00

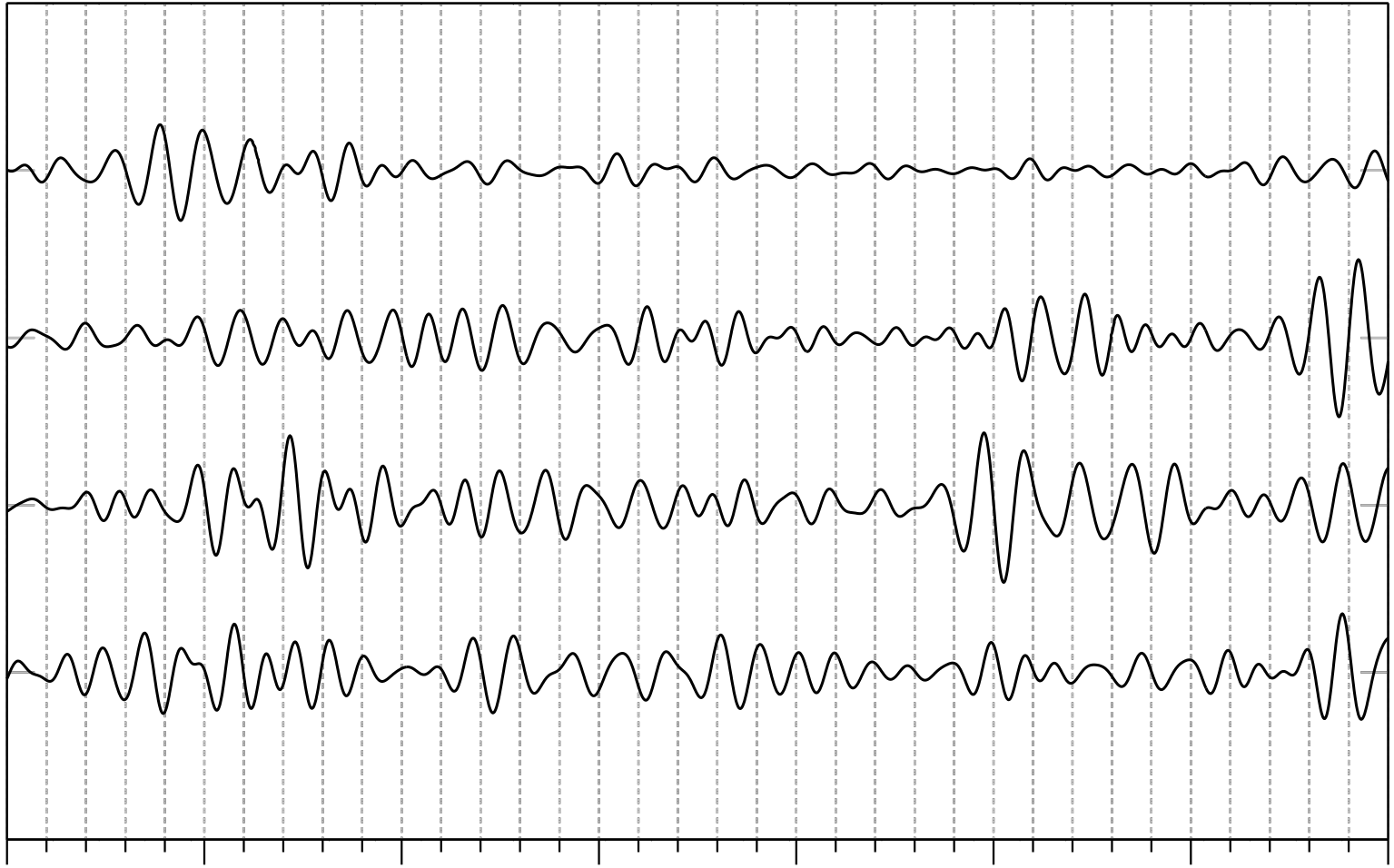
12:10:00

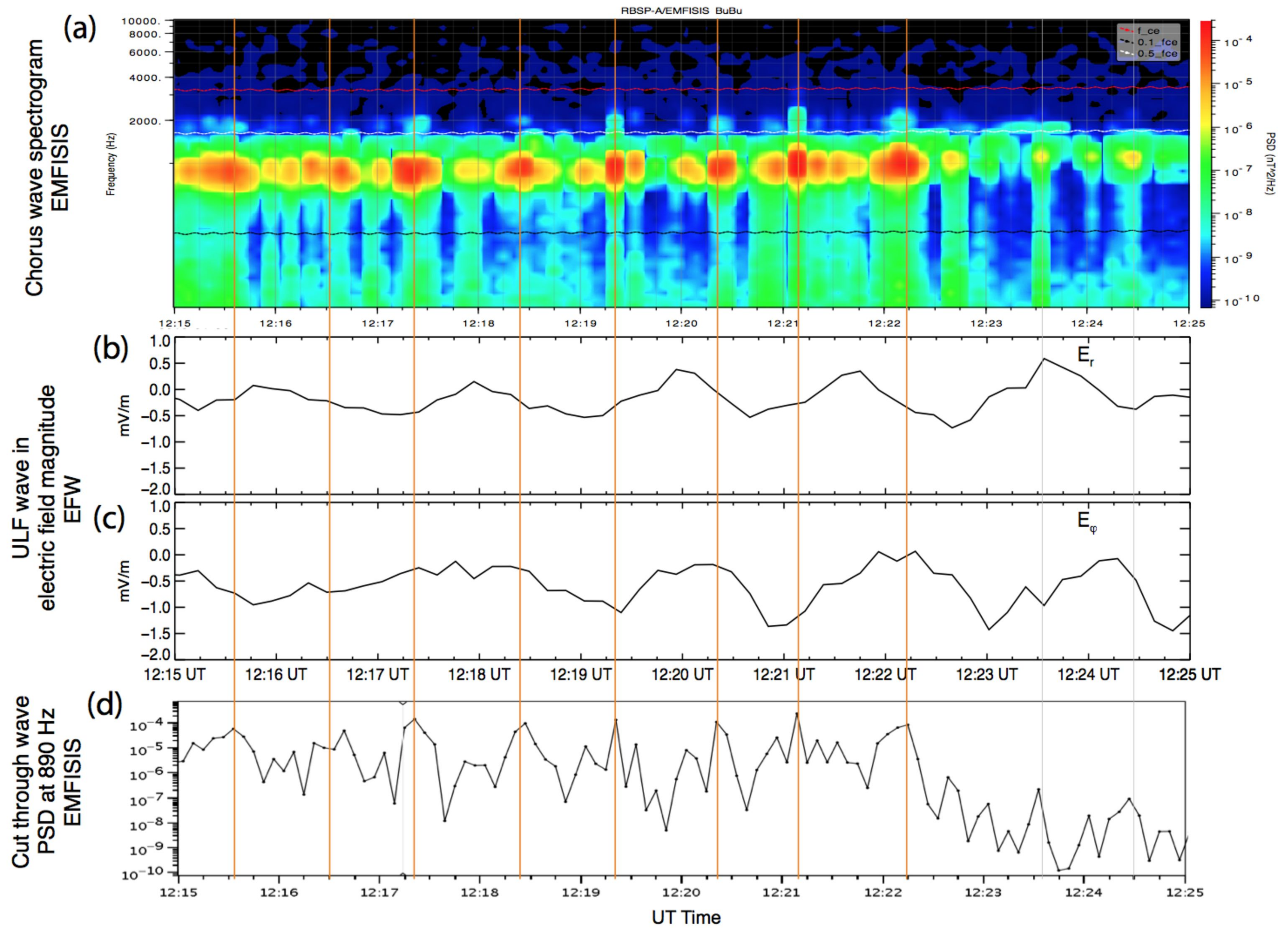
12:15:00

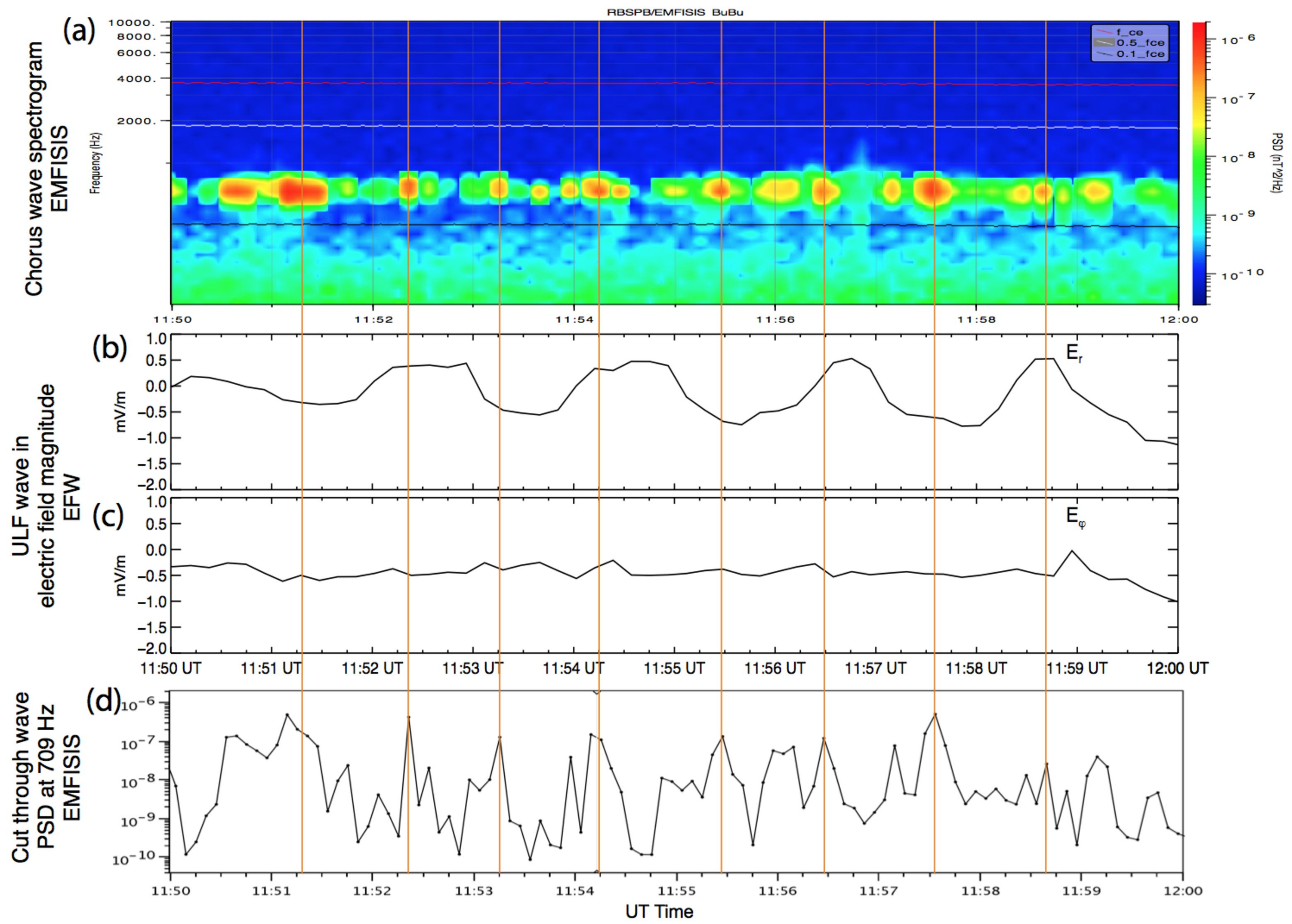
12:20:00

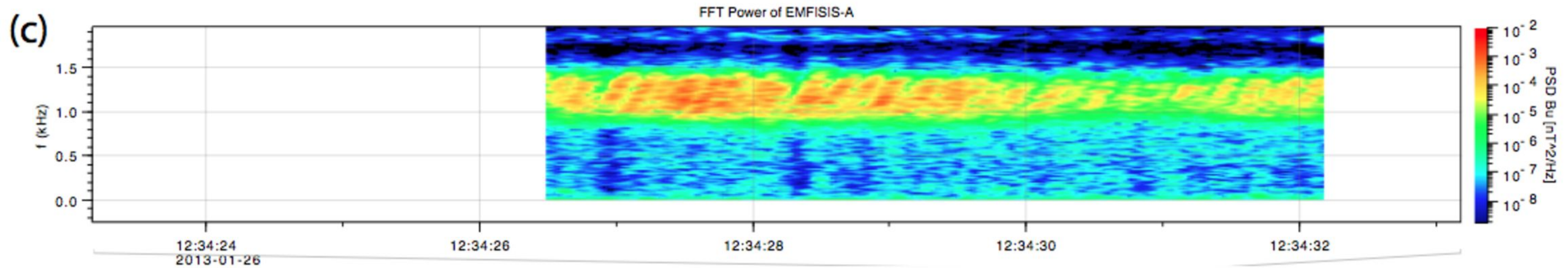
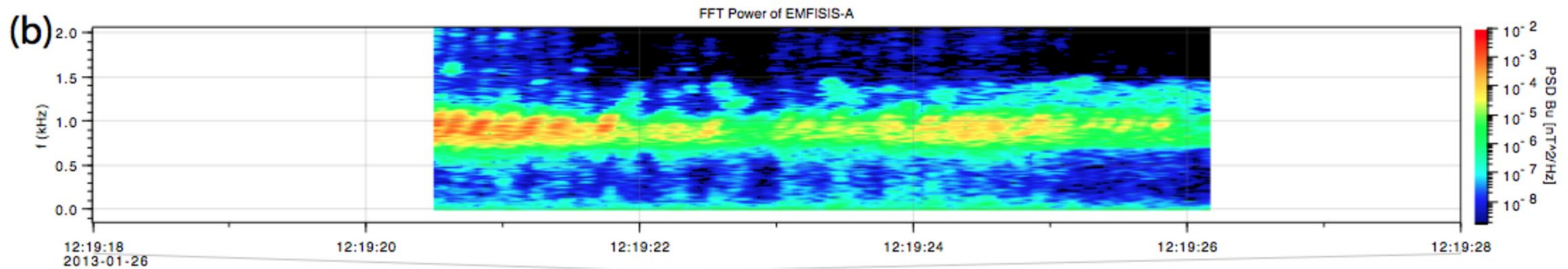
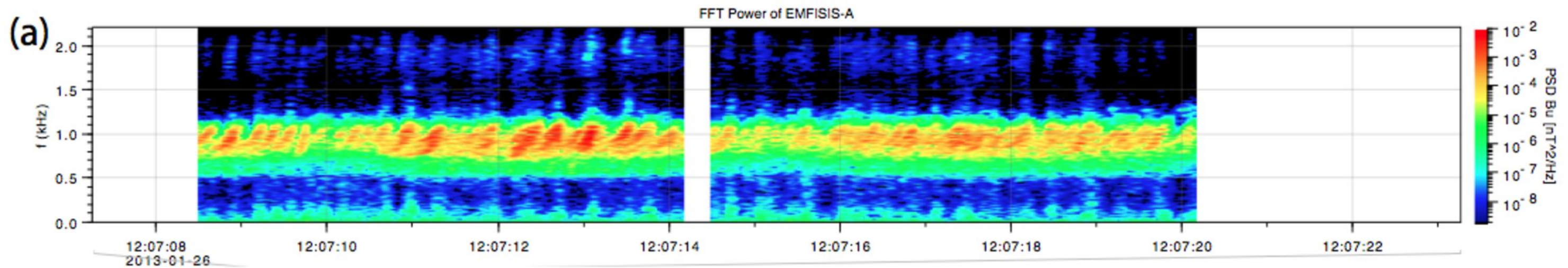
12:25:00

26 Jan 2013









Spectrogram2013-Jan-26 Poker Flat, 557.7 nm (44 fps)

